Impaired dense core vesicle maturation in *Caenorhabditis elegans* mutants lacking Rab2

Stacey L. Edwards,[1] Nicole K. Charlie,[1] Janet E. Richmond,[2] Jan Hegermann,[3] Stefan Eimer,[3] and Kenneth G. Miller[1]

[1]Genetic Models of Disease Program, Oklahoma Medical Research Foundation, Oklahoma City, OK 73104
[2]Department of Biological Sciences, University of Illinois at Chicago, Chicago, IL 60607
[3]European Neuroscience Institute Goettingen, German Research Foundation Research Center for Molecular Physiology of the Brain, 37077 Goettingen, Germany

Despite a key role for dense core vesicles (DCVs) in neuronal function, there are major gaps in our understanding of DCV biogenesis. A genetic screen for *Caenorhabditis elegans* mutants with behavioral defects consistent with impaired DCV function yielded five mutations in UNC-108 (Rab2). A genetic analysis showed that *unc-108* mutations impair a DCV function unrelated to neuropeptide release that, together with neuropeptide release, fully accounts for the role of DCVs in locomotion. An electron microscopy analysis of DCVs in *unc-108* mutants, coupled with quantitative imaging of DCV cargo proteins, revealed that Rab2 acts in cell somas during DCV maturation to prevent the loss of soluble and membrane cargo. In Rab2 null mutants, two thirds of these cargoes move to early endosomes via a PI(3)P-dependent trafficking pathway, whereas aggregated neuropeptides are unaffected. These results reveal how neurons solve a challenging trafficking problem using the most highly conserved animal Rab.

Introduction

Neurons use neuropeptides to initiate and adjust complex behaviors and to modulate signaling via classical neurotransmitters (Scheller and Axel, 1984; Kupfermann, 1991; Kass et al., 2001; Jacob and Kaplan, 2003; Liu et al., 2007; Li and Kim, 2008). Neuronal cell somas use the regulated secretory pathway to package neuropeptides into dense core vesicles (DCVs). This pathway begins in the trans-Golgi, where diverse sorting mechanisms cause neuropeptide precursor proteins (proneuropeptides) and their processing enzymes to coalesce into vesicles that bud from the trans-Golgi to form immature DCVs (for reviews see Arvan and Castle, 1998; Tooze et al., 2001; Borgonovo et al., 2006; Kim et al., 2006). During and after DCV formation, prohormone convertases in the vesicle cleave the proneuropeptides at dibasic residues, and carboxypeptidase E trims off the dibasic residues to produce active neuropeptides (Dikeakos and Reudelhuber, 2007). Aggregation of proneuropeptides facilitates their sorting from other soluble proteins in the trans-Golgi; however, immature DCVs also contain soluble and transmembrane proteins not destined for mature DCVs (for review see Tooze et al., 2001). Studies of endocrine cells have revealed that, after budding from the trans-Golgi, secretory granules (the presumed equivalent of neuronal DCVs) undergo a critical maturation process involving the removal of soluble and transmembrane proteins via clathrin-coated vesicles, which then merge with early endosomes (for reviews see Arvan and Castle, 1998; Tooze et al., 2001). After maturation, neurons use the kinesin motor protein KIF1A to transport mature DCVs along microtubules to axons (Jacob and Kaplan, 2003), where they undergo regulated secretion.

The complexity of DCV biogenesis and maturation presents immense challenges to the membrane trafficking machinery. Although studies of endocrine cells have revealed the aforementioned key insights, little is known about how this process occurs in neurons and the extent to which endocrine cells and neurons use shared or modified trafficking pathways to generate DCVs. Rab proteins are a large family of small GTPases that preserve compartment identity and ensure directionality and specificity during vesicle-mediated transport (Seabra and Wasmeier, 2004; Grosshans et al., 2006). Although studies in PC12 cells indicate that Rab3 and Rab27 are good candidates for assisting with DCV exocytosis (Handley et al., 2007; Graham et al., 2008), Rab

Correspondence to Kenneth G. Miller: millerk@omrf.org

Abbreviations used in this paper: ANF, atrial natriuretic factor; DCV, dense core vesicle; SNP, single nucleotide polymorphism.

The Rockefeller University Press $30.00
J. Cell Biol. Vol. 186 No. 6 881–895
www.jcb.org/cgi/doi/10.1083/jcb.200902095

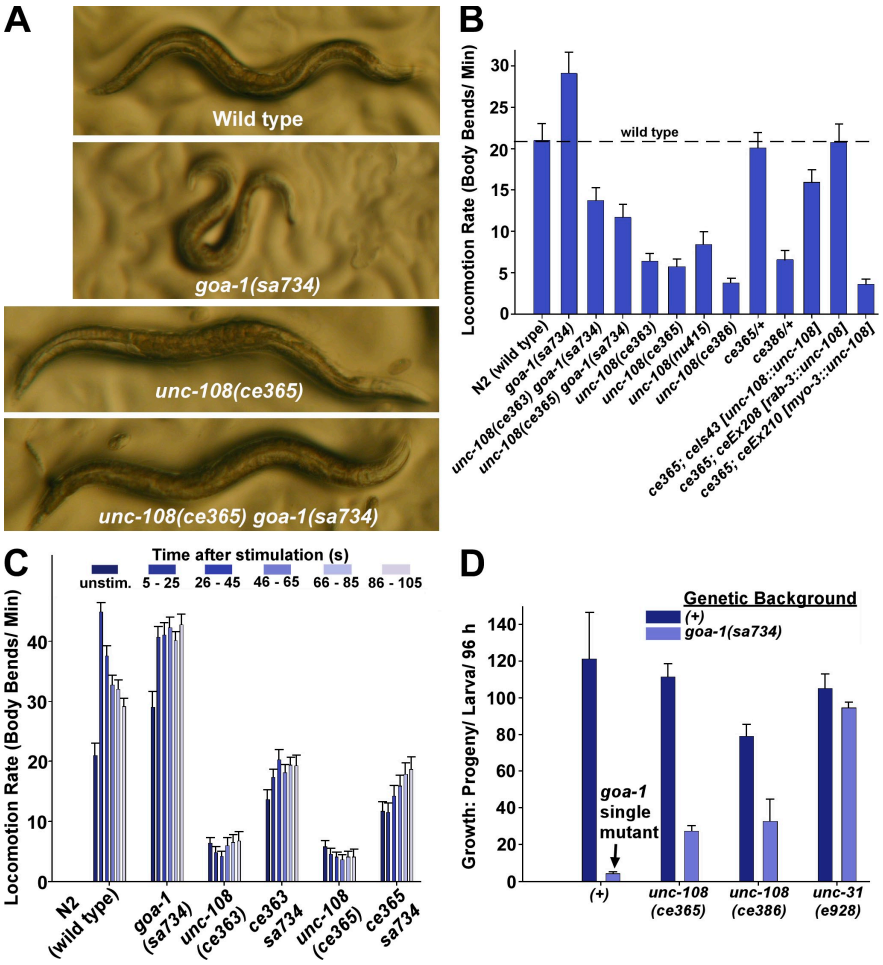

Figure 1. ***unc-108* (Rab2) mutations suppress the hyperactivity and improve the growth of *goa-1(sa734).*** (A) Representative photos with genotypes indicated. Images are scaled identically. Wild-type length is ~1 mm. (B) *unc-108* mutations confer sluggish locomotion in *(+)* and *goa-1* mutant backgrounds. Spontaneous (unstimulated) locomotion rates of N2 (wild type) compared with the indicated genotypes are shown. The last three bars are site of action rescue experiments in which *unc-108* loss-of-function mutants contain transgenes that express the *unc-108* cDNA from the *unc-108* promoter, panneuronally (*rab-3* promoter), or in body wall muscle (*myo-3* promoter). Error bars are SEMs of 10 animals each. (C) *unc-108* single mutants and *unc-108 goa-1* double mutants are sluggish even in response to a harsh stimulus. Locomotion responses of N2 compared with the indicated genotypes at the indicated intervals after a defined mechanical stimulus. Error bars are SEMs of 30 animals each. (D) *unc-108* and *unc-31* mutations improve the growth rate of *goa-1* null mutants. Error bars are the SEMs of three populations of animals plated as first-stage larvae and allowed to grow and produce progeny for 96 h at 20°C.

proteins that function during DCV biogenesis or maturation have not been identified.

Caenorhabditis elegans is ideally suited for the genetic investigation of neuronal DCVs because mutants strongly impaired for DCV function, though nearly paralyzed, are viable (Gracheva et al., 2007; Speese et al., 2007; Hammarlund et al., 2008). In this study, we used a genetic screen to identify a class of *C. elegans* mutants with phenotypes similar to mutants with impaired DCV function. Five of the mutations from this screen disrupted UNC-108 (Rab2). Our genetic analysis showed that Rab2 functions in the same process or pathway as DCVs but is not required for neuropeptide function. The remaining investigation focused on DCV biogenesis and trafficking in Rab2 null mutants. The results revealed that Rab2 acts during DCV maturation in cell somas to prevent the loss of nonneuropeptide luminal and membrane cargo from the vesicles.

Results

A genetic suppressor screen implicates Rab2 in the function of a Gα synaptic signaling network

In *C. elegans*, the GOA-1 ($G\alpha_o$) pathway is the inhibitory pathway for regulating synaptic activity during locomotion. To identify proteins with direct or indirect importance in $G\alpha_o$ synaptic signaling, we performed a genetic screen for mutations that suppress the slow growing, sickly phenotypes and hyperactive behaviors of *goa-1* null mutants. Previous studies showed that the GOA-1 ($G\alpha_o$) pathway exerts its inhibitory effects via the EGL-30 ($G\alpha_q$) pathway (Hajdu-Cronin et al., 1999; Miller et al., 1999). Many of the *goa-1* suppressor mutations mapped either directly to $G\alpha_q$ or to the Rho-specific GEF (guanine nucleotide exchange factor) domain of UNC-73 (Trio), a major $G\alpha_q$ effector (Fig. S1 A; Lutz et al., 2007; Williams et al., 2007). However, one class of suppressors included *unc-31* (CAPS) mutants (Fig. S1 A), which was previously shown to have impaired neuropeptide secretion as the result of a defect in DCV exocytosis (Gracheva et al., 2007; Hammarlund et al., 2007; Speese et al., 2007; Zhou et al., 2007). To identify other proteins that function in DCV trafficking or neuropeptide secretion, we focused on the *unc-31*–like class of *goa-1* suppressor mutants, which can be distinguished from *egl-30* ($G\alpha_q$)–like mutants by phenotypic and genetic interactions (Charlie et al., 2006a).

Genetic mapping revealed that five of the *unc-31*–like *goa-1* suppressor mutations disrupted UNC-108 (Rab2), which is 88% identical to its human orthologue and is the most highly conserved animal Rab (Fig. S1, B and C). A recent study characterized two of these mutations, *ce363* and *ce365*, as recessive, reduction- or loss-of-function mutations resulting in amino acid substitutions at conserved residues (Mangahas et al., 2008).

The images in Fig. 1 A show the extent to which one of the *unc-108* mutations transforms a *goa-1* null mutant with respect to size, body thickness, and posture. The *unc-108* mutations reduced the hyperactive locomotion of *goa-1* mutants to ~50–60% of wild type (Fig. 1 B). A panel of *unc-108* single mutants that included the null deletion mutant *nu415* (Chun et al., 2008) had locomotion rates ~25% of wild type (Fig. 1 B). However, in response to a defined physical stimulus, the locomotion of *unc-108* mutants was only 10% of the wild type–stimulated rate and, unlike that of wild type, remained unchanged after the stimulus (Fig. 1 C). Heterozygous *unc-108(ce365)*/+ and *unc-108(ce363)*/+ animals had locomotion rates not significantly different from wild type (Fig. 1 B and not depicted), showing that these two mutations are recessive; however, *unc-108(ce386)* was dominant, and *ce386*/+ heterozygotes had locomotion rates not significantly different from *ce365* and *ce363* homozygotes (Fig. 1 B). Improving the growth of *goa-1* was the second criterion of the genetic screen. Both dominant and recessive *unc-108* mutations improved the population growth rate of the *goa-1* null approximately six- to eightfold (Fig. 1 D). An *unc-31* null mutation improved *goa-1*'s growth rate >20-fold (Fig. 1 D), thus explaining its strong representation in the suppressor screen along with *unc-108* mutants. The remainder of this study focuses on the recessive, loss-of-function *unc-108* alleles, whereas a separate study analyzes the dominant alleles in more detail (see Sumakovic et al. in this issue).

UNC-108 (Rab2) functions in neurons to control locomotion and is expressed throughout the nervous system

Transgenic site of action experiments showed that driving expression of an *unc-108* cDNA from either its own promoter or a panneuronal promoter rescued the sluggishness of *unc-108* mutants and restored wild-type levels of locomotion, whereas driving expression from a body wall muscle promoter had no effect (Fig. 1 B). A GFP reporter driven by the rescuing *unc-108* promoter was expressed throughout the nervous system (Fig. S2 A). Because we observed expression in all 57 ventral cord motor neurons in adult animals (57.3 ± 0.56 SD; n = 3) and widespread expression in the head and tail ganglia and body neurons, it is likely that UNC-108 is expressed in all neurons. Lower levels of the GFP reporter appeared in nonneuronal cells as well (Fig. S2, B and C). Immunostaining using an antibody raised against recombinant UNC-108 revealed a broad distribution of UNC-108 immunoreactivity in the nervous system (Fig. 2 A). Within neuronal cell somas UNC-108 appeared highly enriched within or surrounding up to several subcellular structures roughly 250–500 nm in diameter (Fig. 2 B). Consistent with previous studies of Rab2 (Short et al., 2001; Sinka et al., 2008), these organelles represent the Golgi apparatus because fluorescently tagged UNC-108 colocalizes with Golgi markers, and Rab2 concentrates in and near the Golgi by immuno-EM (Sumakovic et al., 2009). However, UNC-108 immunoreactivity also appeared nonuniformly throughout the cytoplasm. Immunostaining and immunoblotting comparisons of N2 and the *unc-108(nu415)* null mutant confirmed that the antibody specifically recognizes UNC-108 (Fig. S2, D–F). Imaging of a transgenic strain expressing a GFP–UNC-108 fusion in nine ventral cord motor neurons revealed a distribution similar to that observed by UNC-108 immunostaining. Specifically, most neuronal somas had approximately two areas of concentrated UNC-108 along with other nonuniform areas of less-enriched

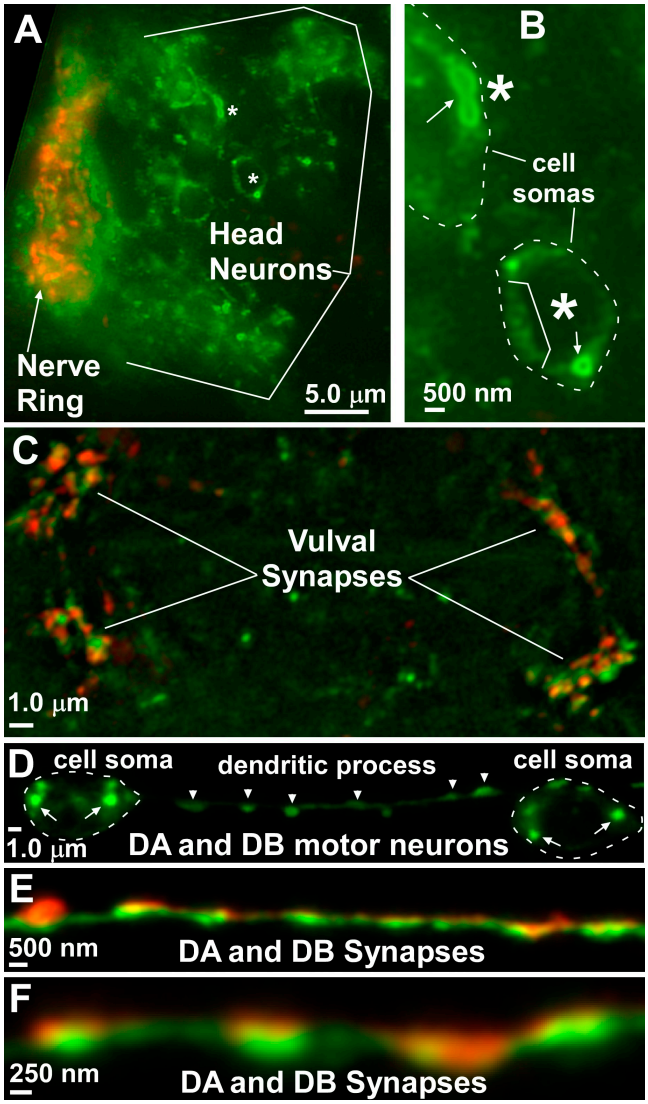

Figure 2. **UNC-108 (Rab2) protein is present in the somas and processes of neurons but is not concentrated at synapses.** (A) The head region of an adult animal is coimmunostained with an antibody against UNC-108 (green) and UNC-17, a cholinergic synaptic vesicle marker (red; Duerr et al., 2001). Asterisks mark cell somas expanded in B. (B) Expanded view of neuronal cell somas from A showing areas of concentrated UNC-108 immunoreactivity in neuronal cell somas. Arrows indicate regions of especially highly concentrated UNC-108 surrounding subcellular structures. The bracketed region indicates lower concentrations of UNC-108 irregularly distributed in the cytoplasm. (C) The vulval region of an adult animal coimmunostained with an antibody against UNC-108 (green) and UNC-17 (red). (D) An N-terminal GFP-tagged version of UNC-108 is highly enriched in small subregions (arrows) within DA6 and DB6 neuronal cell somas. The genotype of the transgene is *ceEx231* [unc-129::GFP–UNC-108, unc-129::RFP–SNB-1]. Arrowheads point to non–Golgi-related GFP–UNC-108 fluorescence in the dendrite. (E and F) GFP-tagged UNC-108 is largely excluded from synaptic vesicle clusters. Two regions of the dorsal cord containing axons of the DA and DB motor neurons. GFP–UNC-108 is green, and synaptic vesicle clusters marked with RFP–SNB-1 (Sieburth et al., 2005) expressed from the same promoter are red.

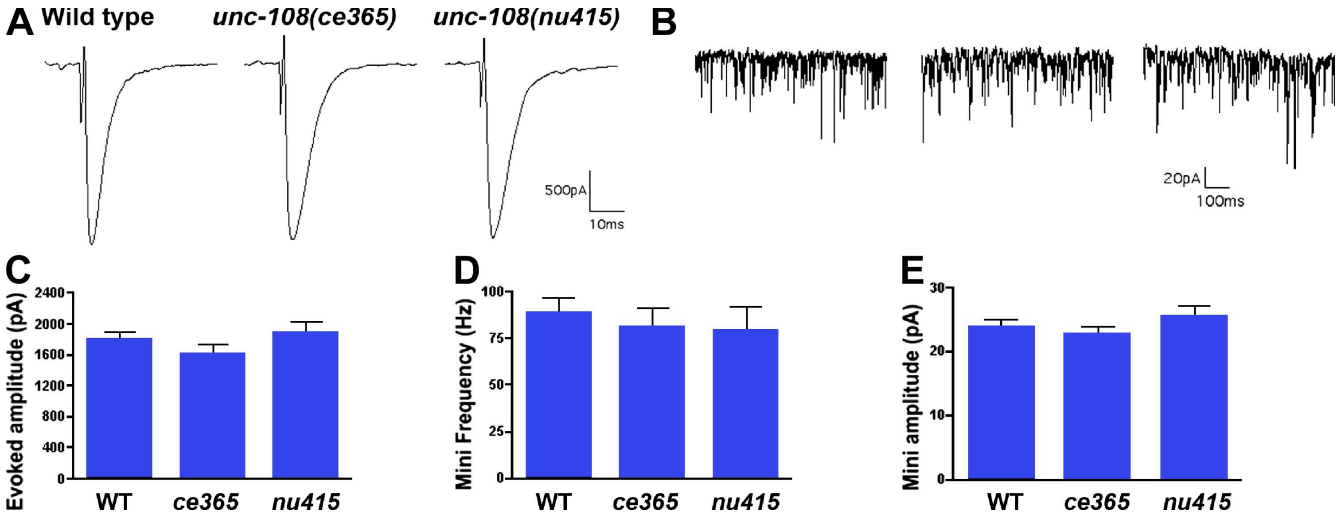

Figure 3. ***unc-108* (Rab2) mutants have normal levels of neurotransmitter release from small synaptic vesicles.** (A) Representative traces of electrically evoked excitatory postsynaptic currents recorded from the body wall muscles of wild type and the indicated *unc-108* mutants. (B) Representative traces of endogenous miniature postsynaptic currents (minis) recorded from the body wall muscles of wild type and *unc-108(ce365)*. (C) Mean amplitude of electrically evoked postsynaptic currents in wild type (WT; $n = 21$), *unc-108(ce365)* ($n = 13$), and *unc-108(nu415)* ($n = 7$). Mann-Whitney p-values of *ce365* and *nu415* versus N2 are 0.096 and 0.6, respectively. (D and E) Mean frequencies and amplitudes of minis recorded from the body wall muscles of wild type ($n = 21$), *unc-108(ce365)* ($n = 13$), and *unc-108(nu415)* ($n = 7$). Mann-Whitney p-values of each mutant versus N2 are all ≥0.4. (C–E) Error bars are SEMs.

UNC-108 (Fig. 2 D). UNC-108 immunoreactivity also coincided with the dense network of axons in the nerve ring (Fig. 2 A). However, imaging larger synapses at higher resolution using both immunostaining and live animal imaging of GFP–UNC-108 showed that it is largely excluded from the synaptic areas of axons (Fig. 2, C, E, and F).

The impaired locomotion of *unc-108* mutants results from functional defects in neurons

In quantitative experiments, the synaptic density of cholinergic synapses in the ventral nerve cord is unaltered in *unc-108* mutants (Fig. S3 A). In addition, the *C. elegans* ultraviolet light response restored greater than wild-type levels of coordinated locomotion to *unc-108* mutants after ∼1 min of illumination with blue-violet light (Fig. S3 B and not depicted). This light response, mediated by the LITE-1 ultraviolet light receptor, largely bypasses the requirement for Gα synaptic signaling pathways in driving locomotion (Edwards et al., 2008). This shows that the impaired locomotion of *unc-108* mutants does not result from permanent developmental defects or permanent damage to neurons, as they develop without UNC-108 (Rab2).

Neurotransmitter release from small synaptic vesicles is normal in *unc-108* mutants

Because *unc-108* affects the function of neurons and is strongly expressed in all 57 ventral cord motor neurons, we used electrophysiological techniques to test whether *unc-108* (Rab2) mutants have defects in the exocytosis of small synaptic vesicles from ventral cord motor neurons (Richmond et al., 1999). Recording from *unc-108(ce365)* and the *unc-108(nu415)* null mutant revealed evoked muscle responses to depolarizing nerve cord stimuli that were not significantly different from wild type (Fig. 3, A and C). Similarly, monitoring endogenous synaptic activity via the miniature postsynaptic currents (minis) that represent the fusion of individual vesicles showed that *unc-108* null mutants have mini frequencies and amplitudes not significantly different from wild type (Fig. 3, B, D, and E). These data show that neurotransmitter release from small synaptic vesicles is unaffected in *unc-108* mutants.

unc-108 (Rab2) mutations disrupt a function of DCVs during locomotion

unc-108 (Rab2) mutants resemble *unc-31* (CAPS) mutants, which have impaired DCV exocytosis (Gracheva et al., 2007; Speese et al., 2007; Zhou et al., 2007; Hammarlund et al., 2008). The phenotypes of *unc-31* null mutants include paralysis under most conditions, slow egg-laying rate, a tendency toward a straight posture on culture plates, the ability to greatly improve the growth of *goa-1* null mutants, and mild resistance to the growth-arresting effects of the acetylcholine esterase inhibitor aldicarb (Fig. 1; Charlie et al., 2006a). *unc-108* null mutants share most of these phenotypes but to a lesser extent when compared with *unc-31* null mutants (Fig. 1; unpublished data).

To test whether *unc-108* and *unc-31* mutations disrupt the same pathway or process, we constructed an *unc-108; unc-31* double null mutant. If the *unc-108* mutation disrupts locomotion by affecting the same process as the *unc-31* deletion, it should not lower the locomotion rate of the *unc-31* null. Consistent with this prediction, the locomotion rate of the *unc-108; unc-31* double null mutant was slightly but significantly higher compared with the *unc-31* single mutant (Fig. 4 A). This contrasts with results using *egl-30* ($G\alpha_q$) reduction-of-function mutants, which have locomotion rates similar to *unc-108* nulls and decrease the locomotion rate of *unc-31* nulls by 36-fold (Charlie et al., 2006a). Because a major role of UNC-31 in *C. elegans* is to promote DCV exocytosis (Gracheva et al., 2007; Hammarlund et al., 2007;

Speese et al., 2007; Zhou et al., 2007), this result suggests that the functions of Rab2 and DCVs overlap during locomotion.

DCV function in neurons is often equated with neuropeptide release. Proneuropeptide processing is required to produce functional neuropeptides. Null mutations in EGL-3 (PC2 convertase) block the cleavage of proneuropeptides at dibasic residues and eliminate most or all of a known set of neuropeptides, as determined by mass spectroscopy of *C. elegans* lysates (Husson et al., 2006); however, it is not clear whether all neuropeptide function is abolished in *egl-3* null mutants. A null mutation in EGL-21 (carboxypeptidase E) disrupts the removal of dibasic residues from PC2-cleaved neuropeptides, which is a required step for producing functional neuropeptides (Jacob and Kaplan, 2003; Husson et al., 2007). The locomotion rates of *egl-3*– and *egl-21* null single mutants were ~25% of wild type and were not significantly different from each other, confirming the important role of neuropeptides in driving locomotion (Fig. 4 A). This is the neuropeptide null phenotype for locomotion because the locomotion rate was not further decreased in *egl-21; egl-3* double null mutants (Fig. 4 A). However, the locomotion rate of *unc-31* null mutants was eightfold lower than *egl-3* null mutants and not significantly different from *unc-31; egl-3* double null mutants (Fig. 4 A). This suggests that EGL-3′s function completely overlaps UNC-31's function but that UNC-31 has one or more other functions unrelated to neuropeptide release.

To determine whether *egl-3* and *unc-108* mutations both disrupt the same neuropeptide-releasing function of UNC-31, we analyzed *unc-108; egl-3* double mutants. The locomotion rates of *unc-108* and *egl-3* single mutants were not significantly different from each other (Fig. 4 A). However, the locomotion rate of *unc-108; egl-3* double null mutants was greatly reduced to a level slightly lower than *unc-31* null mutants (Fig. 4 A). This strong synthetic phenotype suggests that substantial neuropeptide function remains in *unc-108* null mutants. *unc-108; egl-3* double null mutants resemble *unc-31* null single mutants in their overall appearance, posture on culture plates, and response (or lack thereof) to harsh stimuli (Fig. 4 B and Videos 1–5). Together with the other genetic data in Fig. 4, which place both EGL-3 (PC2) and UNC-108 (Rab2) in a locomotion function mediated by DCVs, the similar phenotypes of *unc-108; egl-3* double mutants and *unc-31* single mutants suggest that UNC-108 (Rab2) is required for a DCV-mediated locomotion function that is largely nonoverlapping with neuropeptide release but that, together with neuropeptide release, accounts for the function of DCVs during locomotion.

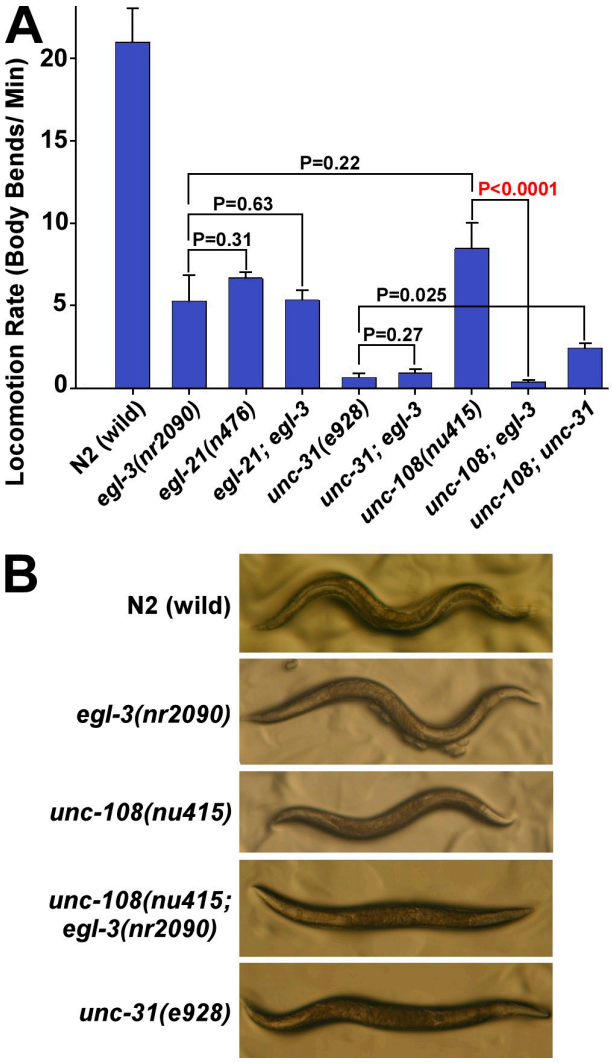

Figure 4. **Genetic analysis suggests that *unc-108* (Rab2) mutations disrupt the trafficking or function of DCVs during the locomotion behavior.** (A) *unc-108* (Rab2) and *egl-3* (PC2) mutations disrupt different functions of UNC-31 (CAPS) in the locomotion behavior. The graph compares the locomotion rates of wild type with the indicated mutants. All alleles are null deletion mutants. Mann-Whitney p-values between the indicated strains are also shown. Error bars are SEMs of 10 animals each. (B) *unc-108; egl-3* double null mutants phenotypically resemble *unc-31* null mutants. Representative adult animals are shown for each genotype. The body length of wild type is ~1 mm, and all images have identical magnification. See also Videos 1–5.

unc-108 (Rab2) mutants have normal numbers of DCVs in their axons

Because the aforementioned genetic analysis implicated UNC-108 in a process mediated by UNC-31 (CAPS) and because UNC-31 mediates DCV exocytosis, we used EM to analyze DCV morphology and numbers in *unc-108(ce365)* mutant axons. The DCVs in this *unc-108* mutant looked similar to wild-type vesicles, having dense cores and mean diameters not significantly different from wild-type DCVs (Fig. 5, A and B). The number of *unc-108* mutant DCVs per unit area within synapses was also not statistically different from wild type (Fig. 5 B). Thus, neither DCV production, as measured by EM, nor transport to axons is impaired in this Rab2 loss-of-function mutant. A related study found similar results for other *unc-108* mutants, including the null mutant *nu415* (Sumakovic et al., 2009).

unc-108 (Rab2) mutants have strongly reduced levels of soluble DCV cargo in their axons

To further investigate which aspect of DCV function *unc-108* mutations disrupt, we analyzed the trafficking of various DCV cargo proteins. We first used the NLP-21 proneuropeptide tagged at its C terminus with the fluorochrome Venus (Sieburth et al., 2007) to follow DCV trafficking in wild-type and *unc-108*

Figure 5. ***unc-108* (Rab2) mutants have normal numbers of DCVs in their axons.** (A) Representative high pressure freezing EM images of wild-type and *unc-108(ce365)* mutant axons. Open arrowheads indicate DCVs; closed arrowheads indicate presynaptic densities. (B) Summary of DCV statistics in wild-type and *unc-108(ce365)* mutant axons. Data are means ± SEMs from the indicated sample sizes. The difference in DCV number between wild type and the *unc-108* mutant is not statistically significant (P = 0.11; Mann-Whitney test).

A

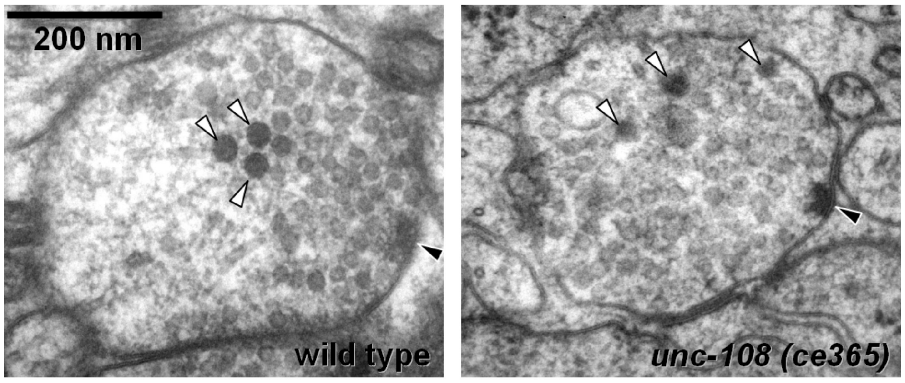

B

Genotype	No. of animals/ synapses/ DCVs analyzed	Number of DCVs/ 0.2 μm²	Average diameter of DCVs (nm)
N2 (wild type)	5/64/128	1.95 +/- 0.20	44.28 +/- 0.59
unc-108(ce365)	4/55/66	1.41 +/- 0.16	43.70 +/- 1.82

mutant live animals. This genomically integrated transgene expresses the tagged propeptide in a set of nine DA/DB ventral cord motor neurons, which allows quantitative imaging of defined axonal and cell soma regions (Fig. S4). Because it is widely accepted that regulated secretory proteins aggregate in the acidic lumen of DCVs (for review see Tooze et al., 2001), we hypothesize that the Venus tag on the propeptide is in an aggregated state in the DCV before peptide processing. After peptide processing, we hypothesize that the NLP-21 neuropeptides remain aggregated, but the Venus tag, now containing only one amino acid from the original propeptide (Nathoo et al., 2001), becomes soluble (Fig. S4). Hereafter, we refer to Venus liberated from the propeptide by peptide processing as soluble Venus or soluble DCV cargo. However, although a peptide processing–induced change in Venus's solubility state is consistent with forthcoming results in this study, such a change remains to be demonstrated at a biophysical level.

A previous study found that a substantial amount of the soluble Venus tag from the NLP-21 propeptide remains within DCVs as they move to axons and is released by an UNC-31–dependent process (Sieburth et al., 2007). When we imaged NLP-21–Venus in the dorsal axons of wild-type animals, we observed concentrated punctal fluorescence along the axons, as previously reported (Fig. 6 A; Sieburth et al., 2007). However, when we crossed this transgenic array into *unc-108* mutants, the NLP-21–Venus levels, although still punctal in nature, were strongly reduced in intensity (Fig. 6, B and C). The integrated fluorescence per micrometer was reduced to ∼25–30% of wild-type levels in a group of three *unc-108* mutants that included the *unc-108(nu415)* null deletion mutant (Fig. 6 F). In contrast, double mutants lacking both Rab proteins involved in DCV exocytosis (Rab3 and Rab27) had higher axonal levels of NLP-21–Venus (126 ± 6.6% of wild type for *aex-6(sa24); rab-3(js49)* double mutants; n = 14 animals each). We also examined the axonal fluorescence of other Venus-tagged neuropeptides in wild-type and mutant backgrounds. Unlike NLP-21, the *C. elegans* neuropeptide FLP-3 is not normally expressed in ventral cord motor neurons (Nathoo et al., 2001; Kim and Li, 2004), and yet FLP-3–Venus still exhibited reduced axonal levels in *unc-108* mutants when compared with wild type (∼37% of the wild-type control; Fig. 6 F). We observed a similar reduction in axonal levels of ectopically expressed Venus-tagged rat atrial natriuretic factor (ANF; ANF-Venus; ∼33% of the *unc-108(+)* control; Fig. 6 F). The impaired trafficking of these DCV cargoes is caused by lack of Rab2 in the neurons expressing the cargo because an *unc-108* null mutant that expresses the *unc-108* cDNA only in the cargo-expressing neurons had wild-type axonal levels of the cargo (Fig. 7, A–C and H).

Blocking neuropeptide processing restores greater than wild-type levels of the neuropeptide tag in *unc-108* mutant axons

The aforementioned data are consistent with at least two possible DCV-related functions that could be disrupted in *unc-108* mutants: (1) trafficking/retention of neuropeptide cargo in DCVs or (2) trafficking/retention of propeptide-derived, nonneuropeptide-soluble cargo in DCVs. We obtained a further clue by examining the delivery of INS-22–Venus to axons in *unc-108* mutants. INS-22 is one of a group of insulins in *C. elegans* that lacks PC2 cleavage sites (Pierce et al., 2001), whereas NLP-21, FLP-3, and ANF all contain multiple PC2 cleavage sites. When we compared INS-22–Venus in *unc-108(+)* and mutant backgrounds, the *unc-108* mutation only reduced its axonal fluorescence to 74% of wild type (Fig. 6, D–F), suggesting that neuropeptide processing affects trafficking of the cleaved Venus tag in *unc-108* mutants. To further test this, we crossed the NLP-21–Venus transgene into *egl-3* null mutants, which cannot cleave proneuropeptides into their constituent peptides. Whereas axonal NLP-21–Venus levels

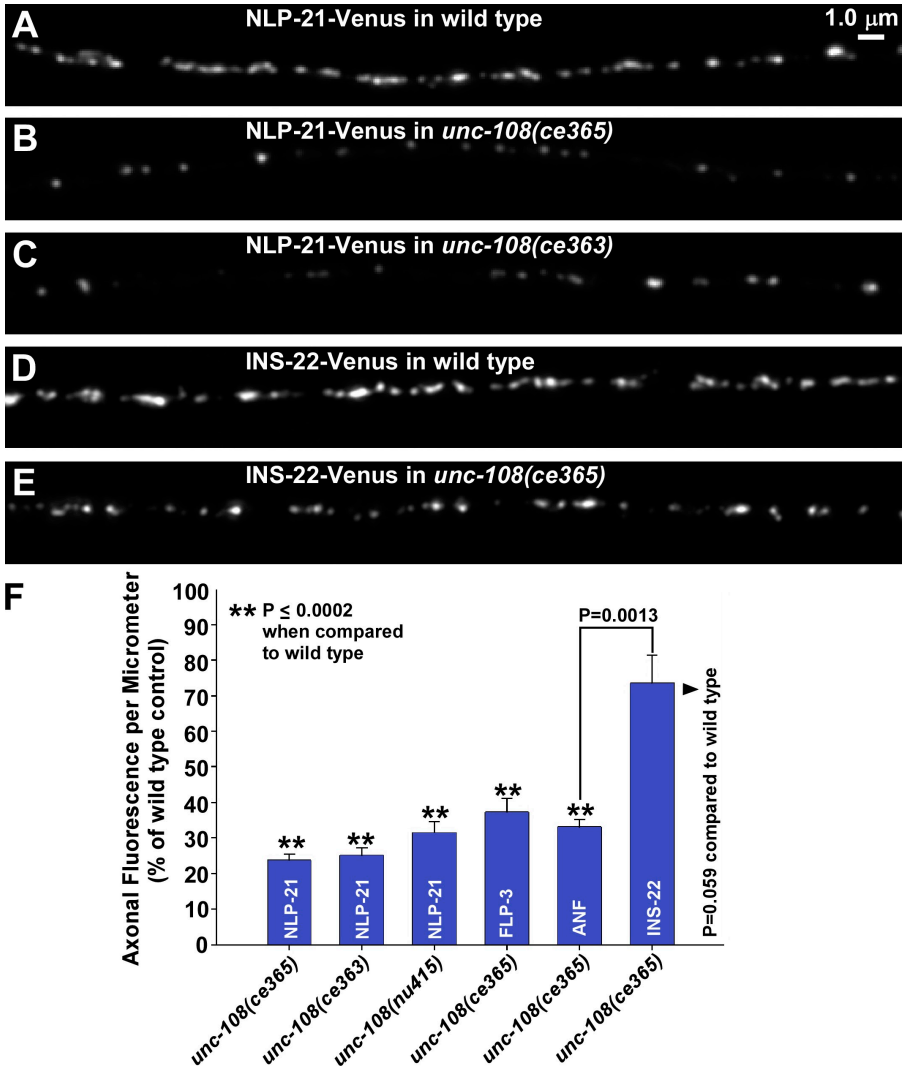

Figure 6. ***unc-108* (Rab2) mutants have strongly reduced levels of PC2-processed Venus cargo in their axons.** (A–E) Representative images of Venus-tagged neuropeptides in DA/DB motor neuron axons in animals with the indicated genetic backgrounds. Strains containing the same transgenic array are scaled identically for brightness after adjusting for differences in light source power. NLP-21–Venus and INS-22–Venus are expressed from the integrated transgenic arrays *nuIs183* and *nuIs195*, respectively. (A–C) UNC-108 is required for normal levels and density of the Venus cargo in axons. (D and E) A peptide tag not cleaved from the proneuropeptide by PC2 convertase is transported to axons in *unc-108* mutants. (F) Quantification of Venus cargo fluorescence in the dorsal axons of *unc-108* mutants. The graph shows the total integrated fluorescence per micrometer of dorsal axon length, expressed as a percentage of the wild-type control, of various tagged neuropeptides in the indicated mutant backgrounds. Data are means and SEMs from images acquired from 6 to 16 individual animals each. NLP-21–Venus, FLP-3–Venus, ANF-Venus, and INS-22–Venus were expressed from the integrated transgenic arrays *nuIs183* (or *celsS6* for *nu415*), *celsS1*, *celsS2*, and *nuIs195*, respectively. P-values are from a Mann-Whitney test and unpaired *t* test with Welch correction.

in *unc-108* null single mutants were only 32% of wild type, this level increased ~4.3-fold in *unc-108; egl-3* double null mutants, to 1.4-fold greater than wild type (Fig. 7, A–E and H). *egl-3* single mutants also had twice as much axonal NLP-21–Venus as wild type (Fig. 7, D and H), suggesting that, in wild type, about half of the soluble Venus cargo is removed from DCVs after peptide processing or that DCVs only partially complete their peptide processing before entering axons and escaping the trafficking pathways that remove soluble proteins. The major conclusion from this series of experiments is that neurons lacking Rab2 lose about two thirds of their soluble Venus cargo after proneuropeptide processing.

Interfering with PI(3)P function restores normal levels of soluble DCV cargo in *unc-108* mutant axons

In pancreatic β cells, clathrin-coated vesicles bud from immature DCVs and carry soluble and transmembrane cargo not destined for mature DCVs to early endosomes, from which their components are either secreted or sent to lysosomes (Turner and Arvan, 2000). PI(3)P is essential for the trafficking of membranes through early endosomes (Di Paolo and De Camilli, 2006; Grosshans et al., 2006; Lindmo and Stenmark, 2006). To determine whether the soluble Venus cargo is lost by a PI(3)P-dependent process in *unc-108* null mutants, we coexpressed NLP-21–Venus and 2XFYVE-RFP, which specifically recognizes PI(3)P and marks early phagosomes and early endosomes in *C. elegans* (Roggo et al., 2002; Yu et al., 2006). 2XFYVE expression has previously been shown to block PI(3)P-dependent processes in DCVs (Meunier et al., 2005). Under these conditions of excess 2XFYVE, we observed no significant difference between wild type and *unc-108* null mutants in the levels or appearance of NLP-21–Venus in axons (Fig. 7, F–H). These data suggest that the reduced axonal levels of the soluble Venus tag in *unc-108* mutants result from its loss by a PI(3)P-dependent membrane trafficking process. Experiments using a dominant-active RAB-5 transgene to block membrane trafficking through early endosomes in *unc-108* mutants produced similar results (Sumakovic et al., 2009).

A trafficking event in neuronal cell somas reduces soluble DCV cargo in *unc-108* mutant axons

Because DCV biogenesis and maturation occur in cell somas, we next examined NLP-21–Venus levels in the cell somas of wild

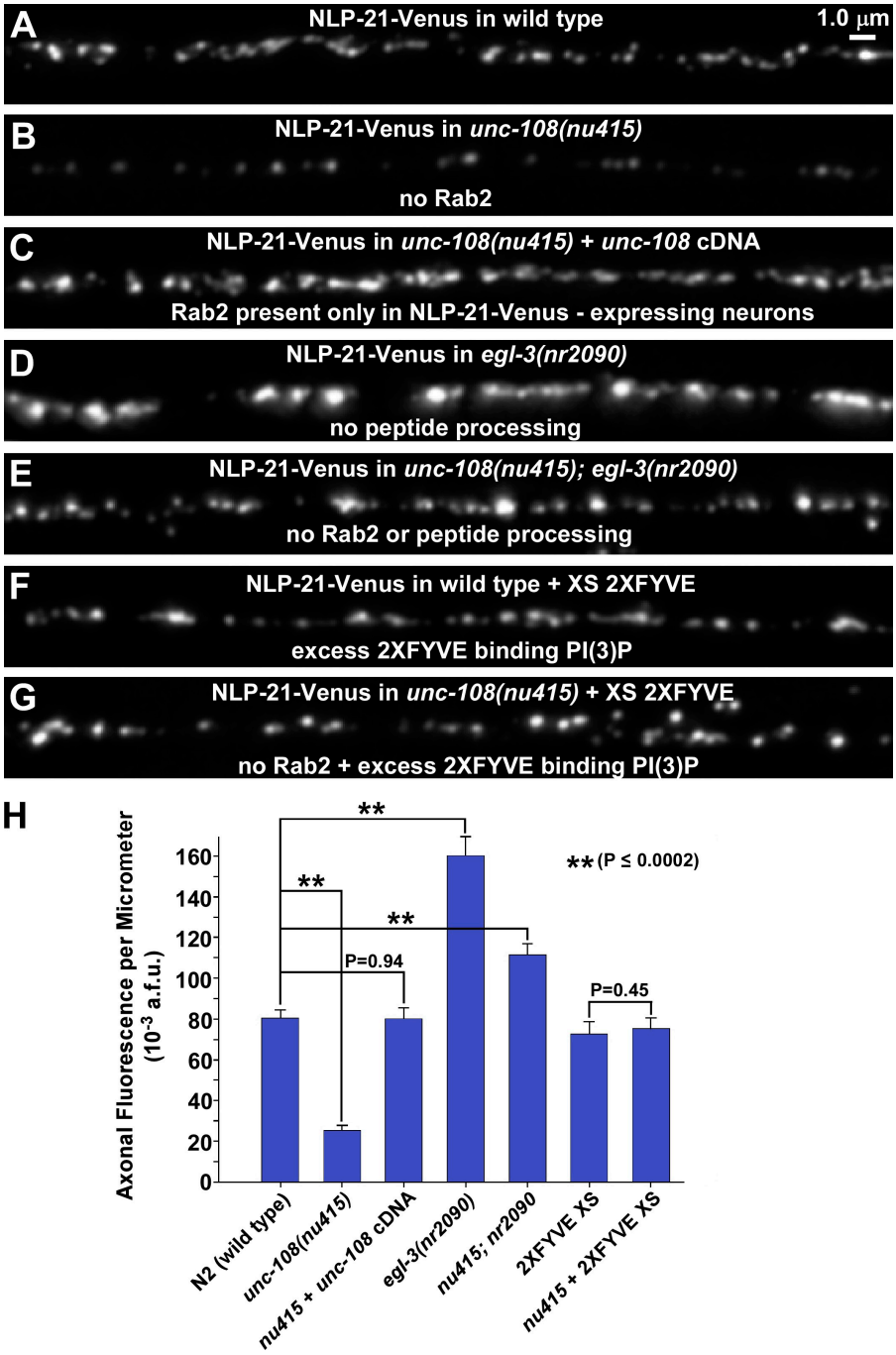

Figure 7. **Blocking neuropeptide processing or PI(3)P restores normal levels of the Venus cargo in *unc-108* mutant axons.** (A–G) Representative images of NLP-21–Venus in DA/DB motor neuron axons in animals with the indicated genetic backgrounds. Strains containing the same transgenic array are scaled identically for brightness after adjusting for differences in light source power. NLP-21–Venus is expressed from the integrated transgenic array *cels56* in A–E and *cels57* in F and G. (A and B) UNC-108 is required for normal levels and density of the Venus cargo in axons. (C) UNC-108 acts cell-autonomously in motor neurons during DCV cargo trafficking. This strain is identical to that in B except that it contains the *ceEx282* transgene, which expresses the *unc-108* cDNA in the same motor neurons as NLP-21–Venus. (D and E) Blocking peptide processing with an *egl-3* (PC2 convertase) null mutation restores greater than wild-type levels of the neuropeptide tag in the axons of wild type and *unc-108* null mutants. (F and G) Blocking PI(3)P function with excess 2XFYVE restores normal levels of the neuropeptide tag in the axons of wild type and *unc-108* null mutants. (H) Quantification of Venus levels in the dorsal axons of *unc-108* mutants. The graph shows the total integrated fluorescence per micrometer of dorsal axon length, expressed as arbitrary fluorescence units (a.f.u.). Data are means and SEMs from images acquired from 11 to 14 individual animals each. NLP-21–Venus was expressed from the *cels56* integrated array for the first five bars and from the *cels57* integrated array for the last two bars. P-values are from the Mann-Whitney test.

type and *unc-108* mutants. In these experiments, we imaged a pair of identified neurons, DA6 and DB6, which are adjacent in the ventral nerve cord (Fig. S4). Each neuron sends a dendrite in the direction of the other neuron, so the images included the dendrites as well. NLP-21–Venus levels in *unc-108* null mutant cell somas were reduced to 57% of the level in wild-type somas (Fig. 8, A, B, and G). Thus, the reduced axonal level of the NLP-21–Venus tag in *unc-108* null mutants results from a trafficking event in cell somas that ultimately results in its degredation or secretion. The trafficking event that removes the Venus tag in *unc-108* mutant somas depends on peptide processing because blocking peptide processing with the *egl-3* null mutation restored NLP-21–Venus levels in *unc-108* mutant somas to ~160% of wild type, only slightly higher than the level in *egl-3* single mutants (Fig. 8, C, D, and G). The trafficking event also depends on PI(3)P because coexpressing 2XFYVE-RFP eliminated the difference between wild type and *unc-108* null mutants with respect to Venus levels in the cell somas (Fig. 8, E–G).

Transmembrane cargo is lost from maturing DCVs in the absence of Rab2

The clathrin-coated vesicles that carry soluble proteins from immature DCVs to the endosomal system are also thought to carry membrane proteins not destined for mature DCVs (Turner and Arvan, 2000; for review see Tooze et al., 2001). To investigate the extent to which aberrant trafficking in *unc-108* mutants

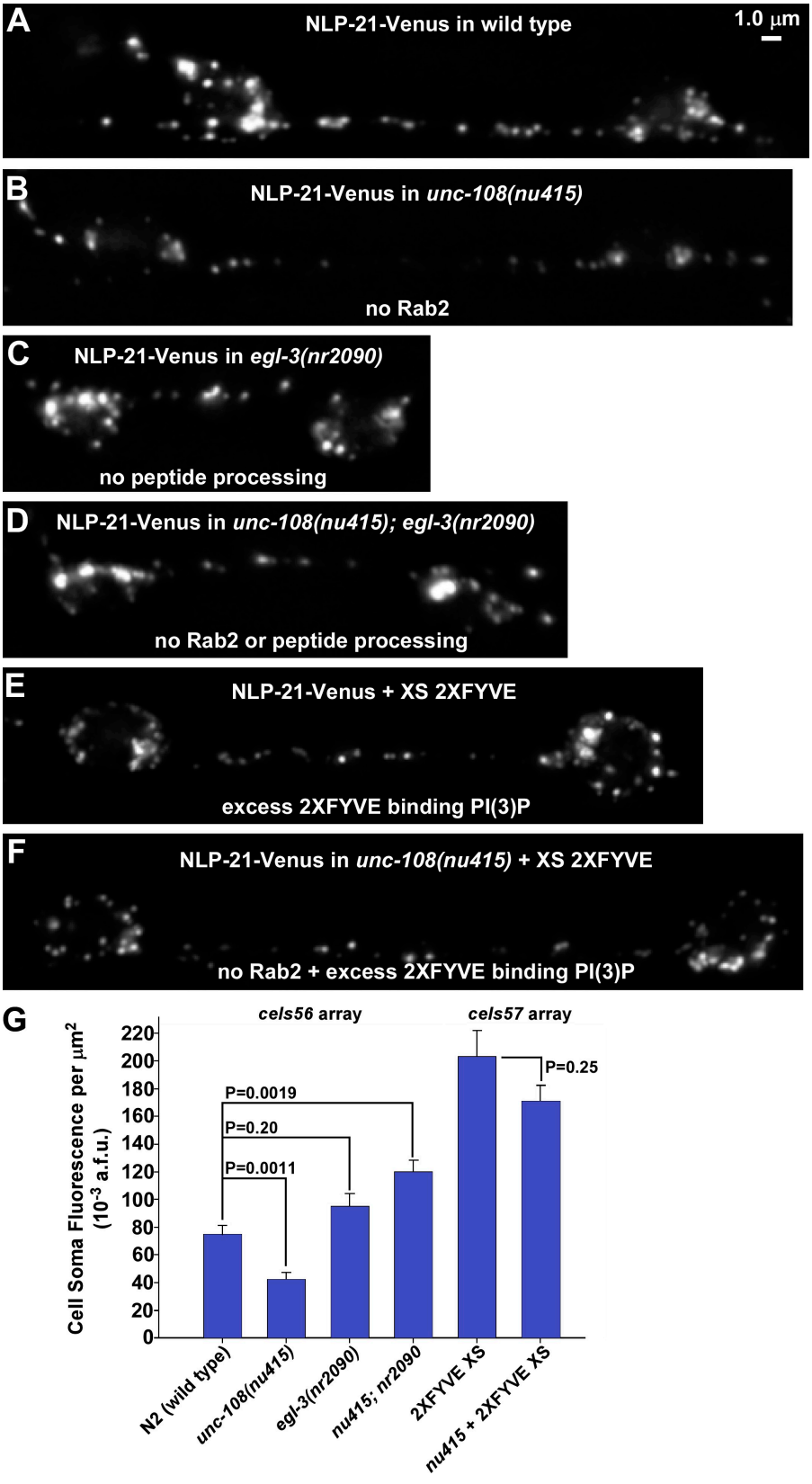

Figure 8. **Blocking neuropeptide processing or PI(3)P restores normal levels of the Venus cargo in *unc-108* mutant cell somas.** (A–F) Representative images of NLP-21–Venus in DA6/DB6 motor neuron cell somas in animals with the indicated genetic backgrounds. Strains containing the same transgenic array are scaled identically for brightness after adjusting for differences in light source power. NLP-21–Venus is expressed from the integrated transgenic array *cels56* in A–D and *cels57* in E and F. DA6 and DB6 neurons show variable spacing. The process between the somas is a dendrite, not an axon. (A and B) UNC-108 is required for normal levels of the Venus cargo in cell somas. (C and D) Blocking peptide processing with an *egl-3* (PC2 convertase) null mutation restores near normal levels of the Venus cargo in the cell somas of *unc-108* null mutants. (E and F) Blocking PI(3)P function with excess 2XFYVE restores normal levels of the Venus cargo in the cell somas of wild type and *unc-108* null mutants. (G) Quantification of Venus cargo levels in the cell somas of *unc-108* mutants. The graph shows the total integrated fluorescence per square micrometer of cell soma and dendrite area, expressed as arbitrary fluorescence units (a.f.u.). Data are means and SEMs from 10 to 15 individual animals each. P-values are from a Mann-Whitney test.

affects the membrane protein composition of mature DCVs, we compared the trafficking of GFP-tagged IDA-1 in wild type and *unc-108* null mutants. IDA-1 is the *C. elegans* orthologue of IA-2 (insulinoma-associated protein 2), a membrane protein specific to DCVs in vertebrate neurons (Solimena et al., 1996), and is a marker for DCVs in *C. elegans* (Cai et al., 2004; Zhou et al., 2007). An integrated IDA-1–GFP transgene showed a punctate localization in wild-type axons that resembled

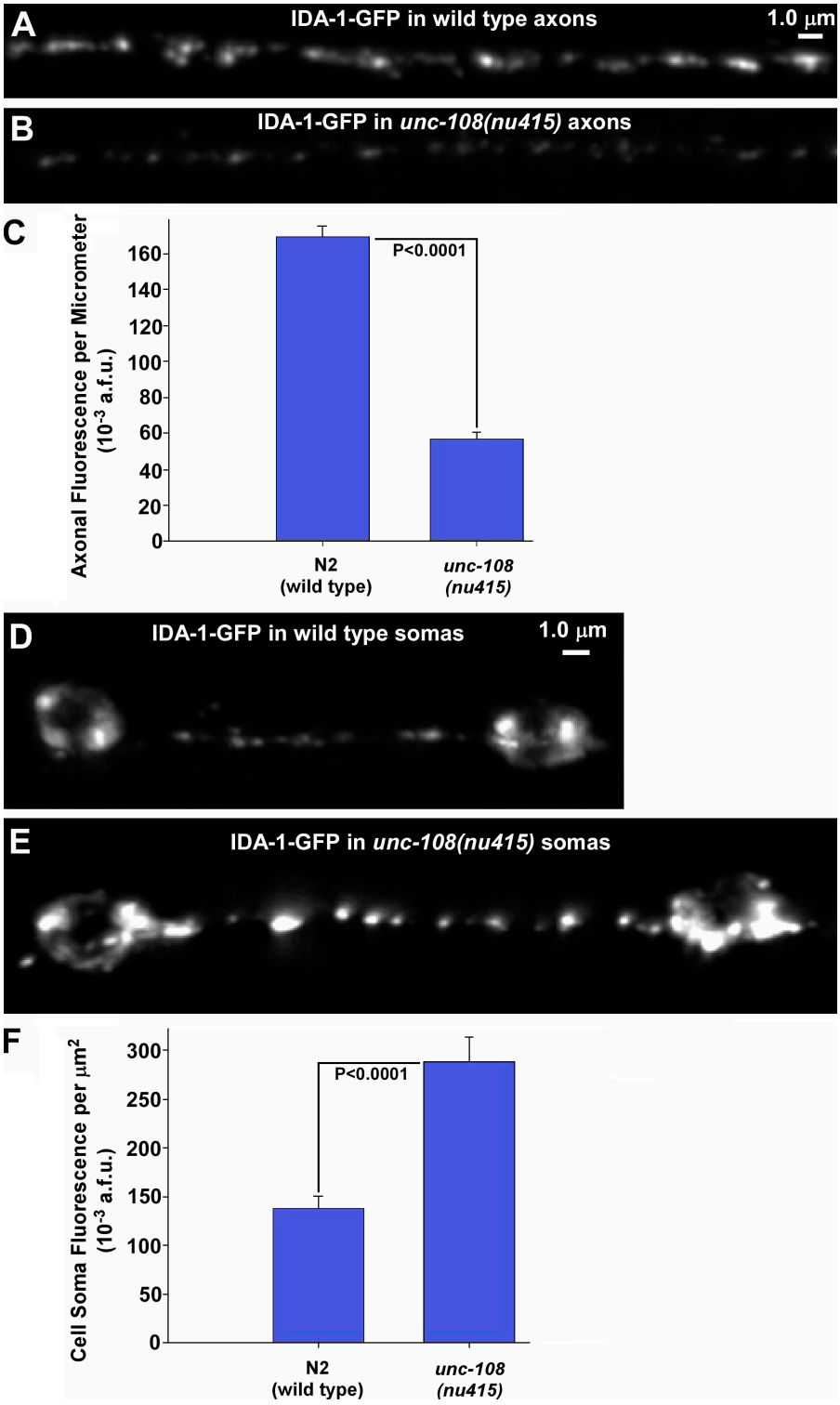

Figure 9. **Transmembrane cargo is lost from maturing DCVs in the absence of Rab2.** (A and B) Representative images of IDA-1–GFP in DA/DB motor neuron axons in wild type (A) and *unc-108(nu415)* (B). Images are scaled identically for brightness after adjusting for differences in light source power. IDA-1–GFP is expressed from the integrated transgenic array *ceIs72*. (C) Quantification of IDA-1–GFP fluorescence in the dorsal axons of wild type and the *unc-108* mutant. The graph shows the total integrated fluorescence per micrometer (arbitrary fluorescence units [a.f.u.]) of dorsal axon length in the indicated backgrounds. (D and E) Representative images of IDA-1–GFP in DA6/DB6 motor neuron cell somas in wild type (D) and *unc-108(nu415)* (E). Images are scaled identically for brightness after adjusting for differences in light source power. (F) Quantification of IDA-1–GFP fluorescence in the DA6/DB6 cell somas of wild type and the *unc-108* mutant. The graph shows the total integrated fluorescence per square micrometer (arbitrary fluorescence units) of cell soma and dendrite area in the indicated backgrounds. (C and F) Data are means and SEMs from 14 animals for each strain. The p-values are from the Mann-Whitney test.

NLP-21–Venus expressed in the same neurons (Fig. 9 A). However, crossing the transgene into the *unc-108* null mutant reduced the axonal levels of IDA-1–GFP to 33% of wild type (Fig. 9, B and C). This level is not significantly different from the extent to which the soluble NLP-21–derived Venus tag is reduced in *unc-108* mutant axons (32%; Fig. 7 G).

Data presented in the previous two sections suggested that the soluble NLP-21–derived Venus tag is trafficked to the endosomal system by a PI(3)P-dependent membrane trafficking process, from which it is likely secreted or sent to lysosomes, as indicated by decreased levels of the Venus tag in *unc-108* mutant somas. The *ida-1* transgene produces IDA-1 tagged with GFP on its cytoplasmic side. Because this GFP tag cannot be secreted or easily broken down by lysosomes, the low axonal levels of IDA-1–GFP in *unc-108* mutants should be associated with higher levels in the cell somas, which is the case.

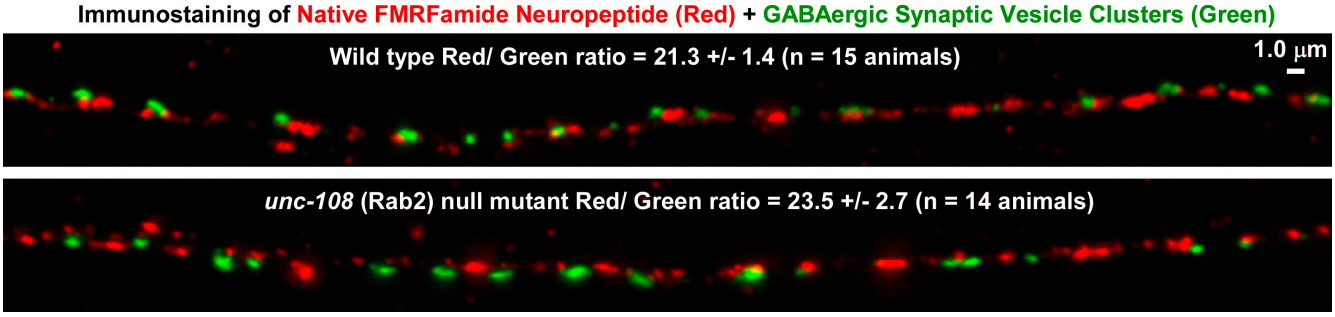

Figure 10. **An *unc-108* (Rab2) null mutant has normal levels of processed FMRFamide neuropeptides in its dorsal nerve cord.** Identically scaled representative images of native FMRFamide neuropeptide and GABAergic synapse immunostaining in the dorsal axons of wild type (top) and the *unc-108(nu415)* null mutant (bottom). The text in each image states the means and SEMs of the FMRFamide/GABAergic synapse fluorescence intensity ratio from 14 to 15 animals per strain. P = 0.98 (Mann-Whitney test). See Materials and methods for further details.

IDA-1–GFP in *unc-108* mutant somas was 200% of its level in wild-type somas (Fig. 9, D–F). This does not precisely compensate for the 300% decrease in *unc-108* mutant axons, which suggests that the cell somas degrade some of the excess IDA-1–GFP or at least its GFP tag. In summary, the IDA-1–GFP data suggest that the same process that depletes the soluble Venus tag from the DCV lumen in cell somas also strips most of the transmembrane cargo IDA-1 from DCVs.

Normal levels of processed neuropeptides in *unc-108* mutant axons

Our finding that propeptide processing makes *unc-108* mutant DCVs vulnerable to losing the soluble Venus tag raises the possibility that processed neuropeptides might also be lost from the mutant's vesicles. If this is true, animals lacking Rab2 should have reduced levels of native, processed neuropeptides in their axons. To test this, we immunostained the mutants with an antibody that recognizes processed FMRFamide neuropeptides in *C. elegans* (Schinkmann and Li, 1992). The levels of native FMRFamide neuropeptides in the dorsal axons of wild type and *unc-108* null mutants were not significantly different (Fig. 10). This is consistent with the genetic analysis showing that substantial neuropeptide function remains in *unc-108* null mutants and the EM analysis showing normal numbers of DCVs in dorsal axons. The FMRFamide immunostaining also suggests that propeptide processing occurs normally in *unc-108* mutant DCVs because in a previous study, disruption of peptide processing strongly affected the ability of this antibody to recognize its substrates in axons (Jacob and Kaplan, 2003).

Discussion

Functional state of DCVs produced without Rab2

Although the DCVs emerging from *unc-108* mutant somas lack two thirds of their transmembrane and soluble cargoes, the EM and FMRFamide-related peptide immunostaining data suggest that they contain normal aggregated neuropeptide cores. Furthermore, blocking peptide processing or attaching the tag to a peptide that lacks processing sites (thus presumably keeping the tag aggregated) prevents its loss. This is not surprising given the aggregated nature of the core, which would not be accessible to membrane trafficking events. In addition to normal levels of aggregated neuropeptides, *unc-108* mutant vesicles contain all of the necessary components for exocytosis, as indicated by coelomocyte uptake assays (Sumakovic et al., 2009), the lack of DCV accumulation by EM, and by our finding that knocking out neuropeptide function strongly decreases the locomotion of an *unc-108* null mutant (i.e., showing that neuropeptides continue to function in *unc-108* mutants). However, our genetic analysis shows that DCVs lacking Rab2 cannot carry out a critical function unrelated to neuropeptide release. Catecholamines can also be packaged into DCVs and, being soluble molecules, would be vulnerable to loss in *unc-108* mutants; however, mutants lacking catecholamines have normal locomotion rates by the assays in this study (unpublished data), so catecholamine release is unlikely to be the missing function. Other possibilities include soluble neurotrophins such as BDNF (brain-derived neurotrophic factor) or NT-3–like proteins, which are known to be released by DCVs (Michael et al., 1997; Mowla et al., 1999; Sadakata et al., 2007), growth factors such as TGF-β that might be secreted by the regulated secretory pathway (Specht et al., 2003), one or more membrane proteins that might use DCVs for transport to synapses such as a G protein–coupled receptor (Guan et al., 2005), or even a membrane domain with a unique phospholipid or lipid–protein composition.

Rab2's specific function during DCV maturation

Previous studies suggested that Rab2 functions in ER to Golgi trafficking based on overexpression of putative dominant-negative Rab2 proteins in cell lines using Golgi-mediated glycosylation of vesicular stomatitis virus G protein as an assay (Tisdale et al., 1992; Tisdale and Balch, 1996). However, a recent study found normal Golgi-mediated glycosylation and anterograde transport of proteins in *C. elegans* neurons lacking Rab2 (Chun et al., 2008). Rab2's strong enrichment in and around the Golgi (Sumakovic et al., 2009) and its direct binding to Golgins and other Golgi-localized proteins (Short et al., 2001; Sinka et al., 2008) seem to suggest a role for Rab2 in a Golgi-specific function. However, light-level immunostaining (this study) and immuno-EM (Sumakovic et al., 2009) showed that Rab2 is also associated to a lesser degree with other compartments around the Golgi, and an earlier study found Rab2 transiently enriched

on newly formed phagosomes, which are essentially early endosomes (Mangahas et al., 2008). Because the Golgi is a major hub for membrane trafficking to and from early endosomes, we favor the idea that Golgins serve to maintain a pool of concentrated Rab2 near its site of action, which, for this function of Rab2, would be immature DCVs near the Golgi and the tubules of early endosomes.

Our study highlights the importance of Rab2 in the DCV maturation process that produces fully functional DCVs in neurons. Much of what we know of DCV maturation comes from studies using nonneuronal cell lines, which may lack the requirement for one or more nonneuropeptide-related DCV functions that are critical for neurons (for reviews see Arvan and Castle, 1998; Tooze et al., 2001; Borgonovo et al., 2006; Kim et al., 2006). In endocrine cells, DCV maturation begins with the synaptotagmin IV–dependent homotypic fusion of immature DCVs (Ahras et al., 2006; for review see Tooze et al., 2001). However, the precise remodeling interactions that occur between homotypically fused vesicles and early endosomes and how these interactions affect mean DCV size, which we found to be unchanged in mutants lacking Rab2, are unknown. Early endosomes are dynamic and often tubulovesicular (Maxfield and McGraw, 2004; Lindmo and Stenmark, 2006). Although maturation uses clathrin-based membrane removal mechanisms, direct interactions between homotypically fused immature DCVs and the tubules of early endosomes have not been ruled out.

The data presented in this study seem to support two hypotheses for Rab2's specific function during DCV maturation. First, Rab2 may speed up a rate-limiting step of the regulated secretory pathway such that DCVs are minimally exposed to early endosomes in the cell soma. If this is the case, Rab2's function in DCV maturation may be similar to its function during phagosome maturation, where it increases the rate of phagosome maturation but is not absolutely required for it (Lu et al., 2008; Mangahas et al., 2008). In a second, equally tenable, hypothesis, Rab2 may inhibit the immature DCV to early endosome trafficking pathway by, for example, limiting the mass or lifetime of early endosomes. Consistent with this possibility, a recent study found an increase in tubulovesicular structures that correspond to early and recycling endosomes in *unc-108* mutant neuronal cell somas (Chun et al., 2008). In a more specific variation of this hypothesis, Rab2 may directly or indirectly regulate the conversion of PI(3)P to other phosphoinositides, much as Rab5 recruits and regulates PI(3) kinase, the enzyme that makes PI(3)P (Di Paolo and De Camilli, 2006; Lindmo and Stenmark, 2006). In this scenario, the absence of Rab2 would lengthen both the lifetime and mass of early endosome tubules, which derive their identity from PI(3)P (Di Paolo and De Camilli, 2006; Lindmo and Stenmark, 2006), thus resulting in excessive interactions between DCVs and early endosomes. Supporting this hypothesis is the finding that *unc-108* mutant phagosomes show a long delay as they mature through the early endosome compartment, and this delay correlates with the persistence of PI(3)P (Mangahas et al., 2008). Thus, as early and recycling endosomes increase in mass or lifetime in animals lacking Rab2, phagosome maturation would slow (Lu et al., 2008; Mangahas et al., 2008), recycling cell surface receptors would accumulate at high levels in the endosomal system (Chun et al., 2008), coelomocytes, having abnormally high endocytic activity, would show impaired trafficking of fluid phase markers (Chun et al., 2008; Mangahas et al., 2008), and maturing DCVs would be vulnerable to assault by early endosomes and loss of their soluble and transmembrane cargo (Sumakovic et al., 2009; this study).

Materials and methods

Worm culture and strains

Worm culture and manipulation essentially followed previously described methods (Brenner, 1974; Stiernagle, 2006), with modifications as described previously (Edwards et al., 2008). In brief, culture media was modified Nematode growth medium, containing no added Ca or Mg, and consisted of the following (per liter): 2 g NaCl, 3.1 g peptone, 3.0 g KH_2PO_4, 0.5 g K_2HPO_4, and 20 g A-7002 agar (Sigma-Aldrich). After autoclaving and cooling to 55°C, the following was added (per liter): 1.6 ml of 5 mg/ml cholesterol in ethanol, 1.0 ml of 100 mg/ml Streptomycin in double distilled H_2O, and 1.25 ml of 10 mg/ml Mycostatin suspension in ethanol. Wild-type worms were the N2 strain. See Table S1 for the complete genotypes of all other strains used in this study.

Forward genetic screens

We mutagenized L4-stage *goa-1* mutants with 1 mM ENU (*N*-ethyl-*N*-nitrosourea) dissolved in ethanol (De Stasio and Dorman, 2001) or 46 mM EMS (ethyl methanesulfonate) in M9 (Sulston and Hodgkin, 1988). We produced synchronous F2 grandprogeny of the mutagenized animals and plated these animals as young larvae on 24-well culture plates using a repeat pipetter to plate ~100 animals in each well for a total of 50,000 F2 animals (ENU) in 2 weekly cycles or 600,000 F2 animals in 10 weekly cycles (EMS). We screened both the F2 and F3 generations on these plates but had the most success in screening the F3 generation, which involved growing the cultures 2 d at RT and 4 d at 20°C after plating. We screened the wells for mutants with improved growth and reduced hyperactive behaviors, including locomotion and egg laying.

Mapping, identification, and outcrossing of suppressor mutations

Suppressor mutants resembling *egl-30*, *unc-31*, *unc-2*, or *unc-73* mutants were complement tested with Dpy-marked versions of these mutants before or after outcrossing from the *goa-1* allele. To map the *unc-108* alleles *ce363* and *ce365*, we first separated the mutations from *goa-1(sa734)* by crossing N2 males to the suppressed strain and isolating putative suppressor single mutants in the F2 generation based on their predicted sluggish phenotype. Animals that were both homozygous for the mutation and did not segregate *goa-1(sa734)* were kept as 1× outcrossed strain stocks. We then produced 5× outcrossed versions of each mutant in *goa-1(+)* and *goa-1(sa734)* backgrounds. During outcrossing, we found tight linkage to the *goa-1* locus on chromosome I. We then mapped the mutations relative to single nucleotide polymorphisms (SNPs) to a 416-kb region centered around −2.0 cM on chromosome I (Fig. S1 B) using a previously described method (Schade et al., 2005). We used the following SNP markers to map the mutations within this region (marker names are followed by genome location, base pair change, and, if relevant, the restriction enzyme that can identify the SNP): *ceP62* [I:3,573,375 (C/T BanII)], *ceP63* [I:4,132,726 (T/A ClaI)], *ceP64* [I:4,663,859 (C/G HinfI)], *ceP194* [3,806,411 (T/A)], and *ceP195* [I: 3,989,632 (G/A)]. We then used candidate gene sequencing of the genomic DNA of each mutant and/or transformation rescue experiments to confirm that all five mutants were *unc-108* alleles.

Plasmids

Table S2 lists all of the plasmids used in this study along with their construction details. In all constructs involving the cloning of PCR fragments, we sequenced the inserts and used clones containing no mutations in the fragment of interest to establish the final plasmid stock.

Transgene production

We produced transgenic strains bearing extrachromosomal arrays by the method of Mello et al. (1991). For all rescue experiments, the original host was *unc-108(ce365)* or *unc-108(nu415); ceIs56*, as indicated. For all other experiments, N2 was the original host. We used pBluescript carrier DNA to bring the final concentration of DNA in each injection mixture to 175 ng/µl

and integrated arrays into the genome as previously described (Reynolds et al., 2005). Table S3 lists all of the transgenic arrays used in this study, their plasmid contents, and the injection concentration of each plasmid.

Live animal assays

The live animal assays have been described in detail in recent studies and were performed in this study without modification: locomotion assays (Miller et al., 1999; Reynolds et al., 2005), stimulated locomotion assays (Charlie et al., 2006b), population growth rate assays (Williams et al., 2007), and light–dark locomotion assays (Edwards et al., 2008). We captured and converted videos of worms on culture plates as previously described (Schade et al., 2005).

Double mutants

We constructed double mutants using the standard method of crossing heterozygous males of mutant A with homozygous hermaphrodites of mutant B and cloning virgin F1 cross progeny. From plates segregating mutant A in their F2 progeny, we cloned mutant A and/or B animals and looked for segregation of the double mutant in the next generation. In some cases, we used PCR to identify plates carrying or homozygous for various deletion alleles. For doubles with transgenes, we cloned candidate doubles directly from the F2 progeny and chose one line homozygous for the fluorescent and behavioral phenotypes in the next generation. For all doubles not involving transgenic arrays, we confirmed the homozygosity of both alleles by PCR and/or sequencing genomic DNA from the final strain.

Electrophysiology

Electrophysiological methods were performed as previously described (Richmond et al., 1999) with the following modifications: ventral body wall muscle cells were recorded in the whole cell voltage-clamp mode (holding potential of −60 mV) using an EPC-10 patch-clamp amplifier (HEKA) and digitized at 1 kHz. The extracellular ~340-mosM solution, pH 7.4, consisted of 150 mM NaCl, 5 mM KCl, 5 mM $CaCl_2$, 4 mM $MgCl_2$, 10 mM glucose, 5 mM sucrose, and 15 mM Hepes. The patch pipette was filled with an ~315-mosM solution, pH 7.2, of 120 mM KCl, 20 mM KOH, 4 mM $MgCl_2$, 5 mM *N*-tris(Hydroxymethyl) methyl-2-aminoethane-sulfonic acid, 0.25 mM $CaCl_2$, 4 mM Na_2ATP, 36 mM sucrose, and 5 mM EGTA. Evoked responses were stimulated with a 2-ms depolarizing pulse delivered via a pipette placed on the anterior ventral nerve cord. Data were acquired using Pulse software (HEKA) and subsequently analyzed and graphed using Pulsefit (HEKA), Mini Analysis (Synaptosoft, Inc.), and Igor Pro (WaveMetrics).

Antibodies, immunohistochemistry, and immunoblotting

To produce the affinity-purified UNC-108 antibody KM32A-3.1, we prepared a recombinant UNC-108 fragment by first transforming KG#303 (GST–UNC-108 [1–212]) into the bacterial expression host BL21(DE3)RIL. We then induced expression of the protein for 17 h at 19°C from a 5-liter culture at an A_{600} of 0.4 using 30 µM IPTG and purified the GST fusion protein over a 5-ml glutathione-agarose column as described previously (Charlie et al., 2006b), except without further purification on an SDS-PAGE gel. Covance then produced a polyclonal antiserum in a goat via a 1,200-µg initial injection and two 600-µg boosts at 3-wk intervals. We affinity purified UNC-108–reactive antibodies by coupling the antigen to an AminoLink Plus column (2-ml bed volume; Thermo Fisher Scientific) according to the manufacturer's instructions. J. Duerr (Ohio University, Athens, OH) and J. Rand (Oklahoma Medical Research Foundation, Oklahoma City, OK) provided the UNC-17 antibody mAb1403 (as mouse monoclonal ascites; Duerr et al., 2001). After preadsorption of the UNC-108 antibody to pure GST on nitrocellulose strips, we coimmunostained wild-type and *unc-108(ce363)* adults for UNC-108 and UNC-17 using methods previously described for other antibodies (Charlie et al., 2006a,b). We used KM32A-3.1 at a 1:400 dilution and mAb1403 at 1:5,000.

We produced the G339.3 UNC-47 antiserum by transforming KG#180 (GST–UNC-47 [1–104]) into the bacterial expression host BL21(DE3). We then induced expression of the protein for 17 h at 19°C from a 5-liter culture at an A_{600} of 0.4 using 30 µM IPTG and purified the GST fusion protein over a 5-ml glutathione-agarose column followed by an SDS-PAGE gel as previously described (Charlie et al., 2006b). Cocalico, Inc. then produced a polyclonal antiserum in a goat via a 1,200-µg initial injection and two 600-µg boosts at 3-wk intervals. We verified the specificity of the UNC-47 antiserum by immunostaining *unc-47(gk192)* (a null mutant), which showed no immunoreactivity at GABAergic synapses using the immunostaining methods and UNC-47 antiserum dilution used in this study. Anti-FMRFamide antiserum 671M (Marder et al., 1987) was a gift from C. Li (City College of New York, New York, NY). We used the anti–UNC-47 and -FMRFamide serums at 1:12,000 and 1:2,000, respectively, after fixing worms for 16 h at 4°C in 4% paraformaldehyde (Schinkmann and Li, 1992). We performed all other steps of freeze-cracking and immunostaining whole mounts of adult animals as previously described (Charlie et al., 2006a,b).

We produced lysates for immunoblotting by producing and isolating ~450,000 eggs per strain. After hatching 18 h at RT on culture plates lacking food, we collected synchronous L1 larvae and counted them by titering. We produced a 300-µl suspension of 1,500 larvae/µl, added an equal volume of 5× SDS-PAGE sample buffer, and immediately froze the suspension in liquid nitrogen. After thawing the suspension in a boiling water bath for 3 min, we passed it three times forcefully through a 26-gauge needle using a tuberculin syringe to produce a lysate. After spinning the lysate for 5 min at 14,000 *g*, we resolved the equivalent of 2,625 L1 lysed larvae of each strain on an 11% SDS-PAGE gel, blotted to nitrocellulose, stained with Ponceau S to visualize molecular mass markers, blocked overnight at 4°C with 3% nonfat dry milk in TBS, and probed the blot with the affinity-purified *unc-108* antibody diluted 1:1,000 for 1 h at RT in TBST (TBS with Tween 20) with 3% nonfat dry milk. Blots were subsequently washed and processed according to the manufacturer's instructions for SuperSignal West Pico (Thermo Fisher Scientific) and exposed to film (BioMax Light; Kodak) to visualize immunoreactive bands.

EM

High pressure freezing and freeze substitution were performed as previously described (Rostaing et al., 2004). A 100-µm-deep aluminum platelet (Microscopy Services) was filled with *Escherichia coli* OP-50 suspension. Approximately 20 young adult worms were transferred into the chamber and immediately frozen using an HPM 10 (BAL-TEC). Freeze substitution was performed in an electron microscope (AFS or AFS2; Leica). For morphological investigations, incubations were at −90°C for 100 h in 0.1% tannic acid and for 7 h in 2% OsO_4 and at −20°C for 16 h in 2% OsO_4, followed by embedding in Epon at RT (all solutions wt/vol in dry acetone). DCVs were quantified from the central profile of each synapse (i.e., from a single EM section for each synapse), and the numbers were normalized to 0.2-μm^2 synaptic profile areas.

Imaging and image analysis

We imaged whole-mounted immunostained adults for UNC-108 and UNC-17 as previously described (Charlie et al., 2006b) using donkey anti–goat and donkey anti–mouse Cy2- and Alexa Fluor 555–labeled secondary antibodies, respectively. We imaged whole-mounted immunostained adults for FMRFamide peptides and UNC-47 GABAergic synaptic vesicle clusters using donkey anti–rabbit and donkey anti–goat Alexa Fluor 555– and Cy2-labeled secondary antibodies, respectively. For quantitative immunostaining, we used the equipment and quantitative imaging techniques described below for live animal imaging. We inferred that dorsal cord immunoreactivity derived from the RID motor neuron axon based on a previous study (Schinkmann and Li, 1992).

We produced live adults for imaging fluorescent-tagged proteins by plating 10–14 L2-stage larvae on each of five locomotion plates (plates were spread with 100 µl of OP-50 bacterial culture and grown for 16 h, lid side up, at 37°C before storing at 4°C) and growing 6 d at 20°C to produce next-generation adult progeny. Approximately 45 young adults were selected and transferred to an unseeded plate, from which we loaded them into a 15-µl drop of 30 mg/ml BDM (2,3-Butanedione monoxime; Sigma-Aldrich; Sieburth et al., 2005) in M9 buffer on a coverslip. After adding another 15 µl of 30 mg/ml BDM, we covered the coverslip and a piece of water-moistened KimWipe with a Petri dish lid. After 10 min, we removed 27 µl of the solution using a P20 microinjection tip (Eppendorf), leaving the worms behind in a small amount of anesthetic. We mounted the coverslip with the worms on a 2% agarose pad (Sulston and Hodgkin, 1988), with the agarose dissolved in M9 buffer. After straightening the coverslip and nudging ~1 mm to help with dorsal/ventral orientation, we sealed each corner with a dab of clear nail polish and imaged animals over the next 35–55 min. In general, two such slides were necessary to obtain images from 14 animals in the correct orientation.

We collected images at 22°C using an inverted microscope (Eclipse TE2000-E; Nikon) equipped with a CFI Apochromat total internal reflection fluorescence 100× NA 1.49 objective (with no additional tube lens or optivar magnification; Nikon), a motorized linear-encoded high resolution z drive (Nikon), a SmartShutter ultrafast shutter (Sutter Instrument Co.) with a Lambda SC controller and a foot pedal switch (Sutter Instrument Co.), and a motorized filter turret containing GFP, CFP, YFP, and

Texas red image–registered filter cubes (Semrock). Our illumination source was an X-Cite illuminator (EXFO), and we captured 12-bit images with a camera (ORCA-AG; Hamamatsu Photonics) controlled by MetaMorph Premier software (version 6.3 r1; MDS Analytical Technologies). To collect images, we scanned the pad using differential interference contrast optics for animals oriented with their ventral or dorsal surfaces facing the objective. We used MetaMorph to acquire a 9-plane image stack z series, with the planes seperated by 0.225 µm. We set MetaMorph to close the SmartShutter between different exposures in the z series. We used 150-ms exposure times for all live animal images, which was well below the saturation limit of the camera chip. We recorded the light source power immediately after every image during imaging using a radiometer (model R5000; EXFO) and then used this data to linearly normalize fluorescence intensities when quantifying images.

To process the images, we used AutoDeblur Gold CWF (Media Cybernetics) to deconvolve the image stacks using the Adaptive PSF (point spread function) blind method and 10 iterations at the low noise setting. After deconvolving, we produced maximum intensity projections of each image stack and adjusted the scaling of wild-type and experimental images to match each other after linearly normalizing for any differences in light source power. We quantified images using MetaMorph Premier (version 6.3 r4), again linearly normalizing the data for light source power for all calculations involving total integrated fluorescence intensities. To normalize the FMRFamide immunostaining to the UNC-47 permeabilization control, we divided the background-adjusted mean FMRFamide intensity per micrometer in the dorsal cord (using a defined region anterior to the vulva) by the background-adjusted mean peak intensity of the four brightest UNC-47 synaptic vesicle clusters in the image, again linearly adjusting for any differences in light source power relative to the reference image.

Online supplemental material

Fig. S1 shows that a genetic screen ties the most highly conserved animal Rab protein to a synaptic signaling function. Fig. S2 shows that *unc-108* (Rab2) is strongly expressed in the nervous system. Fig. S3 shows that *unc-108* mutant phenotypes are not associated with permanent developmental defects or permanently damaged synapses. Fig. S4 shows a model for the physical states of Venus-tagged neuropeptides in DCVs before and after neuropeptide processing. Videos 1–5 show locomotion and harsh touch response of wild-type *C. elegans*, *unc-108(nu415)* mutant, *egl-3(nr2090)* mutant, *unc-31(e928)* mutant, and *unc-108(nu415); egl-3(nr2090)* double mutant, respectively. Tables S1–S3 show the worm strains, plasmids, and transgenic arrays used in this study, respectively. Online supplemental material is available at http://www.jcb.org/cgi/content/full/jcb.200902095/DC1.

We thank Joshua Kaplan, Denise Chun, Zheng Zhou, and Yishi Jin for providing some of the key plasmids and strains we used in this study (indicated in Tables S1 and S2). Janet Duerr and Jim Rand provided the UNC-17 antibody, and Chris Li contributed the anti-FMRFamide serum. Some strains used in this work were provided by the *Caenorhabditis* Genetics Center, which is funded by the National Institutes of Health National Center for Research Resources.

This work was supported by grants from the National Institutes of Health (GM080765 to K.G. Miller and R01 MH073156 to J.E. Richmond) and a grant from the Oklahoma Center for the Advancement of Science and Technology (HR06-078 to K.G. Miller).

Submitted: 18 February 2009
Accepted: 19 August 2009

References

Ahras, M., G.P. Otto, and S.A. Tooze. 2006. Synaptotagmin IV is necessary for the maturation of secretory granules in PC12 cells. *J. Cell Biol.* 173:241–251. doi:10.1083/jcb.200506163

Arvan, P., and D. Castle. 1998. Sorting and storage during secretory granule biogenesis: looking backward and looking forward. *Biochem. J.* 332:593–610.

Borgonovo, B., J. Ouwendijk, and M. Solimena. 2006. Biogenesis of secretory granules. *Curr. Opin. Cell Biol.* 18:365–370. doi:10.1016/j.ceb.2006.06.010

Brenner, S. 1974. The genetics of *Caenorhabditis elegans*. *Genetics*. 77:71–94.

Cai, T., T. Fukushige, A.L. Notkins, and M. Krause. 2004. Insulinoma-associated protein IA-2, a vesicle transmembrane protein, genetically interacts with UNC-31/CAPS and affects neurosecretion in *Caenorhabditis elegans*. *J. Neurosci.* 24:3115–3124. doi:10.1523/JNEUROSCI.0101-04.2004

Charlie, N.K., M.A. Schade, A.M. Thomure, and K.G. Miller. 2006a. Presynaptic UNC-31 (CAPS) is required to activate the $G\alpha_s$ pathway of the *Caenorhabditis elegans* synaptic signaling network. *Genetics*. 172:943–961. doi:10.1534/genetics.105.049577

Charlie, N.K., A.M. Thomure, M.A. Schade, and K.G. Miller. 2006b. The Dunce cAMP phosphodiesterase PDE-4 negatively regulates $G\alpha_s$-dependent and $G\alpha_s$-independent cAMP pools in the *Caenorhabditis elegans* synaptic signaling network. *Genetics*. 173:111–130. doi:10.1534/genetics.105.054007

Chun, D.K., J.M. McEwen, M. Burbea, and J.M. Kaplan. 2008. UNC-108/Rab2 regulates postendocytic trafficking in *Caenorhabditis elegans*. *Mol. Biol. Cell*. 19:2682–2695. doi:10.1091/mbc.E07-11-1120

De Stasio, E.A., and S. Dorman. 2001. Optimization of ENU mutagenesis of *Caenorhabditis elegans*. *Mutat. Res.* 495:81–88.

Di Paolo, G., and P. De Camilli. 2006. Phosphoinositides in cell regulation and membrane dynamics. *Nature*. 443:651–657. doi:10.1038/nature05185

Dikeakos, J.D., and T.L. Reudelhuber. 2007. Sending proteins to dense core secretory granules: still a lot to sort out. *J. Cell Biol.* 177:191–196. doi:10.1083/jcb.200701024

Duerr, J.S., J. Gaskin, and J.B. Rand. 2001. Identified neurons in *C. elegans* coexpress vesicular transporters for acetylcholine and monoamines. *Am. J. Physiol. Cell Physiol.* 280:C1616–C1622.

Edwards, S.L., N.K. Charlie, M.C. Milfort, B.S. Brown, C.N. Gravlin, J.E. Knecht, and K.G. Miller. 2008. A novel molecular solution for ultraviolet light detection in *Caenorhabditis elegans*. *PLoS Biol.* 6:e198. doi:10.1371/journal.pbio.0060198

Gracheva, E.O., A.O. Burdina, D. Touroutine, M. Berthelot-Grosjean, H. Parekh, and J.E. Richmond. 2007. Tomosyn negatively regulates CAPS-dependent peptide release at *Caenorhabditis elegans* synapses. *J. Neurosci.* 27:10176–10184. doi:10.1523/JNEUROSCI.2339-07.2007

Graham, M.E., M.T. Handley, J.W. Barclay, L.F. Ciufo, S.L. Barrow, A. Morgan, and R.D. Burgoyne. 2008. A gain-of-function mutant of Munc18-1 stimulates secretory granule recruitment and exocytosis and reveals a direct interaction of Munc18-1 with Rab3. *Biochem. J.* 409:407–416. doi:10.1042/BJ20071094

Grosshans, B.L., D. Ortiz, and P. Novick. 2006. Rabs and their effectors: achieving specificity in membrane traffic. *Proc. Natl. Acad. Sci. USA*. 103:11821–11827. doi:10.1073/pnas.0601617103

Guan, J.S., Z.Z. Xu, H. Gao, S.Q. He, G.Q. Ma, T. Sun, L.H. Wang, Z.N. Zhang, I. Lena, I. Kitchen, et al. 2005. Interaction with vesicle luminal protachykinin regulates surface expression of delta-opioid receptors and opioid analgesia. *Cell*. 122:619–631. doi:10.1016/j.cell.2005.06.010

Hajdu-Cronin, Y.M., W.J. Chen, G. Patikoglou, M.R. Koelle, and P.W. Sternberg. 1999. Antagonism between $G_o\alpha$ and $G_q\alpha$ in *Caenorhabditis elegans*: the RGS protein EAT-16 is necessary for $G_o\alpha$ signaling and regulates $G_q\alpha$ activity. *Genes Dev.* 13:1780–1793. doi:10.1101/gad.13.14.1780

Hammarlund, M., M.T. Palfreyman, S. Watanabe, S. Olsen, and E.M. Jorgensen. 2007. Open syntaxin docks synaptic vesicles. *PLoS Biol.* 5:e198. doi:10.1371/journal.pbio.0050198

Hammarlund, M., S. Watanabe, K. Schuske, and E.M. Jorgensen. 2008. CAPS and syntaxin dock dense core vesicles to the plasma membrane in neurons. *J. Cell Biol.* 180:483–491. doi:10.1083/jcb.200708018

Handley, M.T., L.P. Haynes, and R.D. Burgoyne. 2007. Differential dynamics of Rab3A and Rab27A on secretory granules. *J. Cell Sci.* 120:973–984. doi:10.1242/jcs.03406

Husson, S.J., E. Clynen, G. Baggerman, T. Janssen, and L. Schoofs. 2006. Defective processing of neuropeptide precursors in *Caenorhabditis elegans* lacking proprotein convertase 2 (KPC-2/EGL-3): mutant analysis by mass spectrometry. *J. Neurochem.* 98:1999–2012. doi:10.1111/j.1471-4159.2006.04014.x

Husson, S.J., T. Janssen, G. Baggerman, B. Bogert, A.H. Kahn-Kirby, K. Ashrafi, and L. Schoofs. 2007. Impaired processing of FLP and NLP peptides in carboxypeptidase E (EGL-21)-deficient *Caenorhabditis elegans* as analyzed by mass spectrometry. *J. Neurochem.* 102:246–260. doi:10.1111/j.1471-4159.2007.04474.x

Jacob, T.C., and J.M. Kaplan. 2003. The EGL-21 carboxypeptidase E facilitates acetylcholine release at *Caenorhabditis elegans* neuromuscular junctions. *J. Neurosci.* 23:2122–2130.

Kass, J., T.C. Jacob, P. Kim, and J.M. Kaplan. 2001. The EGL-3 proprotein convertase regulates mechanosensory responses of *Caenorhabditis elegans*. *J. Neurosci.* 21:9265–9272.

Kim, K., and C. Li. 2004. Expression and regulation of an FMRFamide-related neuropeptide gene family in *Caenorhabditis elegans*. *J. Comp. Neurol.* 475:540–550. doi:10.1002/cne.20189

Kim, T., M.C. Gondré-Lewis, I. Arnaoutova, and Y.P. Loh. 2006. Dense-core secretory granule biogenesis. *Physiology (Bethesda)*. 21:124–133.

Kupfermann, I. 1991. Functional studies of cotransmission. *Physiol. Rev.* 71:683–732.

Li, C., and K. Kim. 2008. Neuropeptides. *WormBook*. 25:1–36. doi:10.1895/wormbook.1.142.1

Lindmo, K., and H. Stenmark. 2006. Regulation of membrane traffic by phosphoinositide 3-kinases. *J. Cell Sci.* 119:605–614. doi:10.1242/jcs.02855

Liu, T., K. Kim, C. Li, and M.M. Barr. 2007. FMRFamide-like neuropeptides and mechanosensory touch receptor neurons regulate male sexual turning behavior in *Caenorhabditis elegans*. *J. Neurosci.* 27:7174–7182. doi:10.1523/JNEUROSCI.1405-07.2007

Lu, Q., Y. Zhang, T. Hu, P. Guo, W. Li, and X. Wang. 2008. *C. elegans* Rab GTPase 2 is required for the degradation of apoptotic cells. *Development*. 135:1069–1080. doi:10.1242/dev.016063

Lutz, S., A. Shankaranarayanan, C. Coco, M. Ridilla, M.R. Nance, C. Vettel, D. Baltus, C.R. Evelyn, R.R. Neubig, T. Wieland, and J.J. Tesmer. 2007. Structure of Gαq-p63RhoGEF-RhoA complex reveals a pathway for the activation of RhoA by GPCRs. *Science*. 318:1923–1927. doi:10.1126/science.1147554

Mangahas, P.M., X. Yu, K.G. Miller, and Z. Zhou. 2008. The small GTPase Rab2 functions in the removal of apoptotic cells in *Caenorhabditis elegans*. *J. Cell Biol.* 180:357–373. doi:10.1083/jcb.200708130

Marder, E., R.L. Calabrese, M.P. Nusbaum, and B. Trimmer. 1987. Distribution and partial characterization of FMRFamide-like peptides in the stomatogastric nervous systems of the rock crab, *Cancer borealis*, and the spiny lobster, *Panulirus interruptus*. *J. Comp. Neurol.* 259:150–163. doi:10.1002/cne.902590111

Maxfield, F.R., and T.E. McGraw. 2004. Endocytic recycling. *Nat. Rev. Mol. Cell Biol.* 5:121–132. doi:10.1038/nrm1315

Mello, C.C., J.M. Kramer, D. Stinchcomb, and V. Ambros. 1991. Efficient gene transfer in *C. elegans*: extrachromosomal maintenance and integration of transforming sequences. *EMBO J.* 10:3959–3970.

Meunier, F.A., S.L. Osborne, G.R. Hammond, F.T. Cooke, P.J. Parker, J. Domin, and G. Schiavo. 2005. Phosphatidylinositol 3-kinase C2alpha is essential for ATP-dependent priming of neurosecretory granule exocytosis. *Mol. Biol. Cell*. 16:4841–4851. doi:10.1091/mbc.E05-02-0171

Michael, G.J., S. Averill, A. Nitkunan, M. Rattray, D.L. Bennett, Q. Yan, and J.V. Priestley. 1997. Nerve growth factor treatment increases brain-derived neurotrophic factor selectively in TrkA-expressing dorsal root ganglion cells and in their central terminations within the spinal cord. *J. Neurosci.* 17:8476–8490.

Miller, K.G., M.D. Emerson, and J.B. Rand. 1999. $G_o\alpha$ and diacylglycerol kinase negatively regulate the $G_q\alpha$ pathway in *C. elegans*. *Neuron*. 24:323–333. doi:10.1016/S0896-6273(00)80847-8

Mowla, S.J., S. Pareek, H.F. Farhadi, K. Petrecca, J.P. Fawcett, N.G. Seidah, S.J. Morris, W.S. Sossin, and R.A. Murphy. 1999. Differential sorting of nerve growth factor and brain-derived neurotrophic factor in hippocampal neurons. *J. Neurosci.* 19:2069–2080.

Nathoo, A.N., R.A. Moeller, B.A. Westlund, and A.C. Hart. 2001. Identification of neuropeptide-like protein gene families in *Caenorhabditis elegans* and other species. *Proc. Natl. Acad. Sci. USA*. 98:14000–14005. doi:10.1073/pnas.241231298

Pierce, S.B., M. Costa, R. Wisotzkey, S. Devadhar, S.A. Homburger, A.R. Buchman, K.C. Ferguson, J. Heller, D.M. Platt, A.A. Pasquinelli, et al. 2001. Regulation of DAF-2 receptor signaling by human insulin and ins-1, a member of the unusually large and diverse C. elegans insulin gene family. *Genes Dev.* 15:672–686. doi:10.1101/gad.867301

Reynolds, N.K., M.A. Schade, and K.G. Miller. 2005. Convergent, RIC-8-dependent Gα signaling pathways in the *Caenorhabditis elegans* synaptic signaling network. *Genetics*. 169:651–670. doi:10.1534/genetics.104.031286

Richmond, J.E., W.S. Davis, and E.M. Jorgensen. 1999. UNC-13 is required for synaptic vesicle fusion in *C. elegans*. *Nat. Neurosci.* 2:959–964. doi:10.1038/12160

Roggo, L., V. Bernard, A.L. Kovacs, A.M. Rose, F. Savoy, M. Zetka, M.P. Wymann, and F. Müller. 2002. Membrane transport in *Caenorhabditis elegans*: an essential role for VPS34 at the nuclear membrane. *EMBO J.* 21:1673–1683. doi:10.1093/emboj/21.7.1673

Rostaing, P., R.M. Weimer, E.M. Jorgensen, A. Triller, and J.L. Bessereau. 2004. Preservation of immunoreactivity and fine structure of adult *C. elegans* tissues using high-pressure freezing. *J. Histochem. Cytochem.* 52:1–12.

Sadakata, T., W. Kakegawa, A. Mizoguchi, M. Washida, R. Katoh-Semba, F. Shutoh, T. Okamoto, H. Nakashima, K. Kimura, M. Tanaka, et al. 2007. Impaired cerebellar development and function in mice lacking CAPS2, a protein involved in neurotrophin release. *J. Neurosci.* 27:2472–2482. doi:10.1523/JNEUROSCI.2279-06.2007

Schade, M.A., N.K. Reynolds, C.M. Dollins, and K.G. Miller. 2005. Mutations that rescue the paralysis of *Caenorhabditis elegans ric-8* (synembryn) mutants activate the $G\alpha_s$ pathway and define a third major branch of the synaptic signaling network. *Genetics*. 169:631–649. doi:10.1534/genetics.104.032334

Scheller, R.H., and R. Axel. 1984. How genes control an innate behavior. *Sci. Am.* 250:54–62.

Schinkmann, K., and C. Li. 1992. Localization of FMRFamide-like peptides in *Caenorhabditis elegans*. *J. Comp. Neurol.* 316:251–260. doi:10.1002/cne.903160209

Seabra, M.C., and C. Wasmeier. 2004. Controlling the location and activation of Rab GTPases. *Curr. Opin. Cell Biol.* 16:451–457. doi:10.1016/j.ceb.2004.06.014

Short, B., C. Preisinger, R. Körner, R. Kopajtich, O. Byron, and F.A. Barr. 2001. A GRASP55-rab2 effector complex linking Golgi structure to membrane traffic. *J. Cell Biol.* 155:877–883. doi:10.1083/jcb.200108079

Sieburth, D., Q. Ch'ng, M. Dybbs, M. Tavazoie, S. Kennedy, D. Wang, D. Dupuy, J.F. Rual, D.E. Hill, M. Vidal, et al. 2005. Systematic analysis of genes required for synapse structure and function. *Nature*. 436:510–517. doi:10.1038/nature03809

Sieburth, D., J.M. Madison, and J.M. Kaplan. 2007. PKC-1 regulates secretion of neuropeptides. *Nat. Neurosci.* 10:49–57. doi:10.1038/nn1810

Sinka, R., A.K. Gillingham, V. Kondylis, and S. Munro. 2008. Golgi coiled-coil proteins contain multiple binding sites for Rab family G proteins. *J. Cell Biol.* 183:607–615. doi:10.1083/jcb.200808018

Solimena, M., R. Dirkx Jr., J.M. Hermel, S. Pleasic-Williams, J.A. Shapiro, L. Caron, and D.U. Rabin. 1996. ICA 512, an autoantigen of type I diabetes, is an intrinsic membrane protein of neurosecretory granules. *EMBO J.* 15:2102–2114.

Specht, H., H. Peterziel, M. Bajohrs, H.H. Gerdes, K. Krieglstein, and K. Unsicker. 2003. Transforming growth factor beta2 is released from PC12 cells via the regulated pathway of secretion. *Mol. Cell. Neurosci.* 22:75–86. doi:10.1016/S1044-7431(02)00023-4

Speese, S., M. Petrie, K. Schuske, M. Ailion, K. Ann, K. Iwasaki, E.M. Jorgensen, and T.F. Martin. 2007. UNC-31 (CAPS) is required for dense-core vesicle but not synaptic vesicle exocytosis in *Caenorhabditis elegans*. *J. Neurosci.* 27:6150–6162. doi:10.1523/JNEUROSCI.1466-07.2007

Stiernagle, T. 2006. Maintenance of *C. elegans*. *WormBook*. 11:1–11.

Sulston, J., and J. Hodgkin. 1988. Methods. *In* The Nematode *Caenorhabditis elegans*. W.B. Wood, editor. Cold Spring Harbor Laboratory, Cold Spring Harbor, NY. 596–597.

Sumakovic, M., J. Hegermann, L. Luo, S.J. Husson, K. Schwarze, C. Olendrowitz, L. Schoofs, J. Richmond, and S. Eimer. 2009. UNC-108/RAB-2 and its effector RIC-19 are involved in dense core vesicle maturation in *Caenorhabditis elegans*. *J. Cell Biol.* 186:897–914.

Tisdale, E.J., and W.E. Balch. 1996. Rab2 is essential for the maturation of pre-Golgi intermediates. *J. Biol. Chem.* 271:29372–29379. doi:10.1074/jbc.271.46.29372

Tisdale, E.J., J.R. Bourne, R. Khosravi-Far, C.J. Der, and W.E. Balch. 1992. GTP-binding mutants of rab1 and rab2 are potent inhibitors of vesicular transport from the endoplasmic reticulum to the Golgi complex. *J. Cell Biol.* 119:749–761. doi:10.1083/jcb.119.4.749

Tooze, S.A., G.J. Martens, and W.B. Huttner. 2001. Secretory granule biogenesis: rafting to the SNARE. *Trends Cell Biol.* 11:116–122. doi:10.1016/S0962-8924(00)01907-3

Turner, M.D., and P. Arvan. 2000. Protein traffic from the secretory pathway to the endosomal system in pancreatic beta-cells. *J. Biol. Chem.* 275:14025–14030. doi:10.1074/jbc.275.19.14025

Williams, S.L., S. Lutz, N.K. Charlie, C. Vettel, M. Ailion, C. Coco, J.J. Tesmer, E.M. Jorgensen, T. Wieland, and K.G. Miller. 2007. Trio's Rho-specific GEF domain is the missing $G\alpha_q$ effector in *C. elegans*. *Genes Dev.* 21:2731–2746. doi:10.1101/gad.1592007

Yu, X., S. Odera, C.H. Chuang, N. Lu, and Z. Zhou. 2006. *C. elegans* Dynamin mediates the signaling of phagocytic receptor CED-1 for the engulfment and degradation of apoptotic cells. *Dev. Cell*. 10:743–757. doi:10.1016/j.devcel.2006.04.007

Zhou, K.M., Y.M. Dong, Q. Ge, D. Zhu, W. Zhou, X.G. Lin, T. Liang, Z.X. Wu, and T. Xu. 2007. PKA activation bypasses the requirement for UNC-31 in the docking of dense core vesicles from *C. elegans* neurons. *Neuron*. 56:657–669. doi:10.1016/j.neuron.2007.09.015